Semi-Hidden Markov Models for Visible Light Communication Channels

Daniel G. Holmes

Declaration

I declare that this dissertation is my own, unaided work, except where otherwise acknowledged. It is being submitted for the degree of Master of Science in Engineering to the University of the Witwatersrand, Johannesburg. It has not been submitted before for any degree or examination to any other university.

Signed this ____ day of _____ 20__

_____
Daniel G. Holmes

Abstract

Visible Light Communication (VLC) is an emerging field in optical wireless communication that uses light emitting diodes (LEDs) for data transmission. LEDs are being widely adopted both indoors and outdoors due to their low cost, long lifespan and high efficiency. Furthermore, LEDs can be modulated to provide both illumination and wireless communication. There is also potential for VLC to be incorporated into future smart lighting systems. One of the current challenges in VLC is being able to deal with noise and interference; including interference from other dimmed, Pulse-Width Modulated (PWM) LEDs. Other noise includes natural light from the sun and artificial light from other non-modulating light sources. Modelling these types of channels is one of the first steps in understanding the channel and eventually designing techniques for mitigating the effects of noise and interference. This dissertation presents a semi-hidden Markov model, known as the Fritchman model, that discretely models the effects of as well as errors introduced from noise and interference in on-off keying modulated VLC channels. Models have been developed for both the indoor and outdoor environments and can be used for VLC simulations and designing error mitigation techniques. Results show that certain channels are able to be better modelled than others. Experimental error distributions shows insights into the impact that PWM interference has on VLC channels. This can be used for assisting in the development of error control codes and interference avoidance techniques in standalone VLC systems, as well as systems where VLC and smart lighting coexist. The models developed can also be used for simulations of VLC channels under different channel conditions.

This work is dedicated to my wife, Camilla, and to my children, Thomas, Benjamin and Carissa.

Acknowledgements

Contents

List of Figures

List of Tables

List of Symbols

The principal symbols used in this dissertation are summarised below, and the first equation in which each symbol appears is given.

SNR	Signal-to-Noise Ratio, *Equation (2.15)*
P_S	Signal power, *Equation (2.15)*
P_B	Background noise power, *Equation (2.15)*
σ^2_{shot}	Shot noise variance, *Equation (2.15)*
$\sigma^2_{thermal}$	Thermal noise variance, *Equation (2.15)*
SINR	Signal-to-Interference-Plus-Noise Ratio, *Equation (2.16)*
P_I	Interference power, *Equation (2.16)*
$\mathbf{A}$	State transition matrix, *Equation (3.1)*
a_{ij}	Transition probability from state i to j, *Equation (3.1)*
N	Number of states, *Equation (3.1)*
$\mathbf{B}$	Error generation matrix, *Equation (3.2)*
b	Error generation probability, *Equation (3.2)*
$\mathbf{\Pi}$	Initial state probability matrix, *Equation (3.3)*
π_i	Initial state probability, *Equation (3.3)*
Γ	Fritchman model parameters, *Equation (3.7)*
$\overline{O}$	Error sequence, *Equation (3.8)*

α_t — Forward variables, *Equation (3.9)*

β_t — Backward variables, *Equation (3.10)*

$\zeta_t(i,j)$ — Expected number of transitions from i to j, *Equation (3.16)*

$\gamma_t(i)$ — Expected number of transitions from i, *Equation (3.17)*

e_k — Error state at position k, *Equation (3.19)*

C_t — Scaling constant, *Equation (3.20)*

σ_B^2 — Background noise variance, *Equation (A.3)*

σ_{PWM}^2 — PWM signal variance, *Equation (A.3)*

σ_S^2 — Signal variance, *Equation (A.4)*

Nomenclature

2D   **2**-**D**imensional

3D   **3**-**D**imensional

5G   **5**th **G**eneration mobile networks

ADC   **A**nalogue-to-**D**igital **C**onverter

AWGN   **A**dditive **W**hite **G**aussian **N**oise

BER   **B**it-**E**rror **R**ate

BSC   **B**inary **S**ymmetrical **C**hannel

CDMA   **C**ode-**D**ivision **M**ultiple-**A**ccess

CIR   **C**hannel **I**mpulse **R**esponse

COTS   **C**ommercial-**o**ff-**t**he-**S**helf

DC   **D**irect **C**urrent

DECT   **D**igital **E**nhanced **C**ordless **T**elecommunications

DPSK   **D**ifferential **P**hase-**S**hift **K**eying

DS/SSMA   **D**irect-**S**equence **S**pread-**S**pectrum Multiple-**A**ccess

EFRD   **E**rror-**F**ree **R**un **D**istribution

FDM   **F**requency **D**ivision **M**ultiplexing

FoV   **F**ield-**o**f-**V**iew

fps   **f**rames **p**er **s**econd

GE   **G**ilbert-**E**lliot

GSM   **G**lobal **S**ystem for **M**obile

HMM   **H**idden **M**arkov **M**odel

HMGM   **H**idden **M**arkov **G**enerative **M**odel

IEEE   **I**nstitute for **E**lectrical and **E**lectronics **E**ngineers

IID   **I**ndependent and **I**dentially **D**istributed

IM/DD   **I**ntensity **M**odulation with **D**irect **D**etection

IoT   **I**nternet **o**f **T**hings

IR   **I**nfra-**R**ed

ISI   **I**nter-**S**ymbol **I**nterference

kbps   **K**ilobits **p**er **s**econd

LED   **L**ight **E**mitting **D**iode

Li-Fi   **Li**ght **Fi**delity

LoS   **L**ine-**o**f-**S**ight

LTE   **L**ong **T**erm **E**volution

Mbps   **M**egabits **p**er **s**econd

MIMO   **M**ultiple-**I**nput and **M**ultiple-**O**utput

MM   **M**arkov **M**odel

MSE   **M**ean **S**quared **E**rror

OFDM   **O**rthogonal **F**requency **D**ivision **M**ultiplexing

OLED   **O**rganic **L**ight **E**mitting **D**iodes

OOK   **O**n-**O**ff **K**eying

OWC   **O**ptical **W**ireless **C**ommunication

PDP   **P**ower **D**elay **P**rofile

PHY   **Ph**ysical layer

PSK   **P**hase-**S**hift **K**eying

PWM   **P**ulse **W**idth **M**odulation

QPSK   **Q**uadrature **P**hase-**S**hift **K**eying

RMS	**R**oot **M**ean **S**quare
SDR	**S**oftware **D**efined **R**adio
SHMM	**S**emi-**H**idden **M**arkov **M**odel
SINR	**S**ignal-to-**I**nterference-Plus-**N**oise **R**atio
SNR	**S**ignal-to-**N**oise **R**atio
TIA	**T**rans**i**mpedance **A**mplifier
USRP	**U**niversal **S**oftware **R**adio **P**eripheral
V2I	**V**ehicle-to-**I**nfrastructure
V2V	**V**ehicle-to-**V**ehicle
VHF	**V**ery **H**igh **F**requency
VLC	**V**isible **L**ight **C**ommunication
Wi-Fi	**Wi**reless **Fi**delity

Chapter 1

Introduction

Light emitting diodes (LEDs) are rapidly being adopted as part of the next generation of lighting systems. This is due to their high efficiency, longer lifespan and low cost. They are used for both indoor and outdoor lighting, as well as for auto-mobiles. LEDs also form part of smart lighting devices and networks. Another advantage of LEDs is that they have the ability to transmit information. Their light can be modulated in such a way that variations in intensity is imperceptible to the human eye. Thus, LEDs can provide both illumination and wireless data transmission, which is known as Visible Light Communication (VLC) [1, 2].

The electromagnetic spectrum that is currently being used for wireless communication has become crowded and bandwidth is expensive. Another challenge is that the demand for wireless connectivity is growing at an increasing rate. This is due to growth in areas such as the Internet of Things (IoT) and 5th generation mobile networks (5G) [3]. VLC has the potential to help meet or supplement the growing demand for wireless connectivity, particularly in last mile access. VLC is a relatively new field and research is taking place to make VLC become part of future wireless communication systems.

One of the challenges for VLC is providing reliable communication in the presence of noise and interference within the visible light spectrum. One of the initial steps in mitigating the noise and interference is modelling these effects and the impact they have on communication in the visible light spectrum. In general, there has been few works on VLC channel modelling. This research focuses on discrete channel models for indoor and outdoor vehicle-to-vehicle (V2V) VLC. Discrete channel models are favourable because they are computationally more efficient compared to waveform channel models [4]. With the physical aspects of the signal abstracted, the signal can be characterised in terms of a small set of parameters. Until now, there have been no

symbol level discrete channel models for VLC reported in literature. A semi-hidden Markov model (SHMM) proposed by Fritchman can be used for discrete channel modelling of a digital channel [5]. The Fritchman model has been used in the past to provide a statistical distribution of errors in wireless channels, particularly channels with bursty errors. These models are also able to simulate error sequences with error patterns comparable to real channels.

The parameters of such models are found by expectation maximisation using the Baum-Welch algorithm [6]. Error sequences obtained from experiments are used as input data for the Baum-Welch algorithm to train the models. Once the parameters for the models are found, the models are used to simulate channel error sequences. A statistical model for channel errors can help in the design of error control codes, interference avoidance and mitigation in future smart lighting and V2V communication systems, and as part of VLC system software simulations. Additionally, the Fritchman model can provide a better distribution of channel errors than a single bit error rate (BER) value.

1.1   Problem Statement

Noise and interference which can potentially cause errors in a VLC channel come from a variety of sources. This includes both natural light and artificial light, both modulated and unmodulated. In the outdoor environment, artificial light sources typically include lights from vehicles, buildings, housing, billboards and street lamps [7]. In the indoor environment, artificial light sources typically include ceiling lights, which can be incandescent, fluorescent or even LED bulbs [1, 8]. The complete transition from older indoor lighting to LED technology is still taking place. Therefore, early VLC systems may be deployed in environments where non-LED lighting still exists. Furthermore, the potential co-existence of VLC with smart lighting systems [2] presents a unique challenge where non-transmitting lighting levels become more dynamic. An example of this would be if an LED is pulse width modulated (PWM) with varying duty cycles for different dimming levels.

For this dissertation, the research question is:

What is the statistical distribution of error states for smart lighting indoor VLC and outdoor V2V VLC channels, from differing scenarios of noise and interference, based on semi-hidden Markov models?

1.2   Research Motivation and Significance

In order to realise the full potential of VLC, the effects of noise and interference need to be understood. More especially, these need to be understood in terms of different scenarios. Practical implementations of VLC systems will be used in a variety of environments. Thus, models based on experimental data under environmental conditions are favourable. For the purposes of this research, it includes outdoor and indoor environments, as well as indoor smart lighting environments.

The potential impact of this research is the following:

1. The results of this research can potentially show opportunities for research into future VLC smart lighting systems and V2V VLC, such as interference avoidance and mitigation techniques.

2. The channel models developed may be used to help design VLC error control codes, or be used for high level simulations of VLC channels under differing noise and interference scenarios, both indoor and outdoor.

3. To the best of the author's knowledge, this is the first work that uses SHMM for modelling of optical communication systems reported in literature.

4. It is also the first work to report the impact of smart lighting on a VLC system based on experimental data.

5. Potential submission of two papers to academic journals; one paper based on the indoor research and the other based on the outdoor research.

1.3   Scope and Objectives

Since VLC is a candidate for last mile wireless connectivity, the main practical application is indoor VLC. This is where VLC is able to broadcast to users in homes and offices and supplement the wireless downlink demand. Additionally, smart lighting would be typically employed indoors. As such, the first focus of the research is in an indoor environment that contains fluorescent lights as well as natural light from the sun that comes through the windows. As far as experiments for the indoor environment is concerned, it is limited to a lab environment with a fixed position. A dynamic VLC receiver is not considered in this research. Furthermore, the lab environment does not contain a smart lighting system. Thus, a single smart lighting

LED had to be included as part of a test bed which does limit the scope in terms of the smart lighting aspect of the research. The first objective is to obtain experimental data from the indoor VLC environment.

The other promising use case of VLC is in V2V communication in the outdoor environment. Newer auto-mobiles use LEDs for their front and rear lights. These LEDs can be used to transmit data. In order to limit the scope, the outdoor VLC modelling is slightly different to the indoor, even though Fritchman models are still used. The outdoor modelling includes only a receiver (or sensor) and the noise and interference is modelled based on sensing the outdoor environment and not on actual transmissions. This is because it is assumed that noise is additive and can still be modelled without transmissions. Thus, the second objective is to obtain experimental data for the outdoor environment. Part of achieving these objectives includes the design and construction of hardware for collection of experimental data. The impact of only modelling through sensing is that the channel models are potentially more general to outdoor VLC, as opposed to the indoor models that consider particular modulation techniques.

The next objective is to use the data collected to analyse error distributions to develop the Fritchman models. This is done by using the Baum-Welch algorithm. The models from the indoor channels are used to generate new models and simulate the channels. These new models can generate error sequences of their own and are then compared to the experimental error sequences. The final objective is to analyse these models mathematically and determine their performance and how well they fit the experimental data.

1.4   Dissertation Organisation

The dissertation is organised as follows:

Chapter 2 gives a literature review which contextualises the rest of the research presented. The first section is an overview of VLC. This provides an overview of some of the technical aspects of VLC systems, including general VLC system requirements, typical transmitters and receivers, modulation techniques and VLC applications. This section is necessary in order to appreciate some of the design of the experimental hardware presented in later chapters. The next sections of the literature review present aspects of the VLC IEEE standard relative to the V2V part of the VLC research. Following that is a review of general channel models that are commonly

used in VLC research. The rest of Chapter 2 is devoted to current literature on indoor and outdoor VLC channel modelling, smart lighting, the Baum-Welch algorithm and the Fritchman model.

Chapter 3 provides a description of the related techniques. The chapter gives details on Markov models, the Fritchman model and the Baum-Welch algorithm. This includes much of the mathematical aspects of these techniques. Details on the evaluation criteria and error probabilities of the models are also given.

Chapter 4 presents the research on indoor channel modelling which is based on a paper currently under review for submission to a journal. Details are given of the different modelling scenarios or cases that were investigated. The design of the indoor VLC transmitter, receiver and smart lighting LEDs are given. The experimental procedure is outlined. A large part of this chapter is then devoted to the results and the discussion.

Chapter 5 presents the research on the outdoor V2V channel modelling. Firstly, the difference in approach between indoor and outdoor modelling is given. Similarly, the sensing system design is presented within the context of the IEEE VLC standard. The experimental procedure is outlined. A section on results and discussion is also given.

Chapter 6 is the concluding chapter in which a research summary is given, along with recommendation for possible future work, followed by a final conclusion.

Chapter 2

Literature Review

2.1 VLC Overview

2.1.1 Basic Indoor VLC Requirements

One of the benefits of indoor VLC is that the existing light infrastructure can be used for downlink data transmission in an optical wireless communication (OWC) system. However, the modulation of the communication signal should be able to coexist with the constant illumination. This means that there should be no visible flickering and the dimming of lights, if required, should also be able to take place. IEEE 802.15.7 is the current standard for VLC. It is currently not finalised, but does include some specifications for modulation schemes and dimming support [9].

2.1.2 Transmitter

White light for VLC can be produced by using either of the following below. It should be noted that maximum transmission speeds attained and reported in literature vary depending on the modulation technique and the transmission distance:

1. **Blue LED with Phosphor**: This is the most common white LED where the semiconductor is blue, but the yellow phosphor coating on the outside of the LED results in a white light being emitted. The phosphor coating does limit the transmission bandwidth of these types of LEDs [1], however transmission speeds of up to 340 Mb/s have been achieved, at a distance of up to 43 cm [10].

2. **RGB LED**: Not only does the combination of the RGB colours produce the white light, but it can also be used for colour-shift keying (CSK) [11, 12, 13]. One of the most recent high speeds achieved using RGB LEDs for VLC was a data rate of 3.22 Gbit/s at a distance of 25 cm [14].

2.1.3   Receiver

VLC signals can be received by either of the following:

1. **Photodetector (photodiode)**: This receiver simply converts the received light into electrical current. The use of a photodetector was reported in one of the very first publications on VLC [15] and is now used regularly. These photodetectors typically have a bandwidth in the order of tens of MHz [1].

2. **Camera sensor**: This consists of a large number of photodetectors. Most mobile phones include a CMOS camera which is convenient for use as a VLC receiver as no additional external hardware needs to be added to the mobile phone [16]. However, the best current phone cameras are limited by up to 1000 fps [17]. In order to improve these speeds, the rolling shutter effect of these cameras has been exploited to provide data rates multiple times faster than the standard camera frame rate [18, 19].

2.1.4   Modulation Techniques

VLC channel connections can be either line-of-sight (LOS) or diffuse. The diffuse connections are as a result of the reflections of light off walls or other objects [20]. VLC modulation is referred to as being Intensity Modulated/Direct Detection (IM/DD).

On-Off keying (OOK) is the simplest modulation technique that can be used for VLC. The bandwidth of this modulation technique is limited by the response time of the LED, which is only several MHz for regular LEDs. There are several pulse modulation methods which also exist, which include variations on PWM and pulse position modulation (PPM).

OFDM has the advantage over other modulation methods in that it can reduce the amount of inter-symbol interference (ISI) and the effects of multipath fading. Higher transmission rates can also be achieved with OFDM; however, it does have more implementation complexity. Because CSK modulation doesn't use white LEDs,

modulation is not limited by the yellow phosphor coating. It can also achieve higher transmission rates in cases where other modulation methods are unable to support the dimming requirement. In CSK, modulation takes place by varying the intensity of the red, green and blue colours [1].

2.1.5 Existing Prototyping Hardware

OpenVLC is an open source prototyping platform currently being used in the VLC community. The board includes a BeagleBone Black which is run by a Linux operating system, with a software defined implementation. At the PHY layer it implements OOK modulation, with a photodetector as the receiver. The advantage of OpenVLC is that it can be used for rapid prototyping. However, it is limited by the fact that it can provide only OOK modulation [21]. Some other Software Defined Radio (SDR) implementations make use of Universal Software Radio Peripherals (USRPs). These have the advantage of flexibility in terms of the modulation techniques that can be employed for VLC, yet the USRPs are less suitable for rapid prototyping as they tend to be more expensive [22].

A front end implementation designed to be used with low cost boards was used in [23]. This gives a 360° coverage using 20 LEDs and provides the flexibility of being able to use either a Raspberry Pi, BeagleBone, or an Arduino as the VLC backend. An Arduino was also used in [24] for an indoor positioning system that uses VLC and ultrasound.

2.1.6 Applications

One of the foremost and promising applications is the integration of VLC and Wi-Fi to form what is known as Li-Fi. This would typically be used in the office or home environments where there is existing LED lighting infrastructure. The VLC component would supplement the Wi-Fi downlink. There is also an added security benefit with such a system as the light signals cannot penetrate through walls, making it more difficult for interception of communication signals [25]. VLC has also been used for indoor localisation which exploits the use of existing lighting infrastructure [26, 27]. VLC has also been used in conjunction with power-line communication [28] and has been applied to indoor environments such as hospitals [29].

Another VLC application that has received a lot of attention is in the automotive

space. LED lights already present on the front and back of motor vehicles can be used for communication between neighbouring motor vehicles or between vehicles and nearby infrastructure such as traffic lights [30]. VLC has also been used for underwater communication [31].

2.1.7   Smart Lighting

Another benefit of the adoption of LEDs for lighting is the potential it has for smart lighting systems. These systems promise even further energy and cost savings. This is in addition to the energy savings from LEDs. This is because smart lighting systems can assist in providing optimal usage. The intelligence embedded within these proposed smart lighting systems can potentially be used in conjunction with VLC [2] [32].

2.2   IEEE 802.15.7 Standard for VLC

The IEEE is in the process of developing a standard for short range optical communication using visible light (IEEE 802.15.7) [9]. The work on the standard thus far includes support for three modulation schemes and three PHY layers. The modulation schemes include OOK, variable pulse position modulation (VPPM) and CSK. The three PHY layers are:

- PHY I: low data rate applications (hundreds of kbps) using OOK and VPPM for outdoor usage.

- PHY II: moderate data rate applications (tens of Mbps) using OOK and VPPM for indoor usage.

- PHY III: moderate data rate applications (tens of Mbps) for CSK applications with multiple light sources and detectors.

Figure 2.1 shows the spectral regions that each of these layers occupy. PHY I has clock rate operating modes of 200 kHz and 400 kHz. PHY II and III have an overlap in their spectral regions between operating clock modes of 3.75 MHz up to 120 MHz. The different PHY layers are able to coexist by using frequency division multiplexing (FDM), except for PHY II and III which have a significant overlap. The standard has
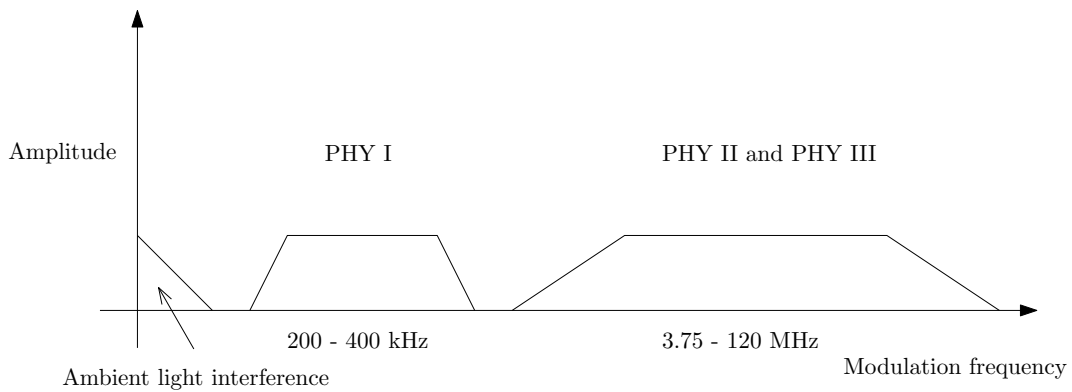
Figure 2.1: PHY layer frequencies for modulation as per IEEE 802.15.7 - 2011 [1]

the PHY I layer higher on the frequency spectrum than most ambient light spectrum. This is in an effort to reduce the ambient light noise and interference.

2.3   General Channel Models

There are two approaches modelling a channel behaviour. The first is applying a signal level approach where the channel is modelled in terms of signal parameters. These would typically include models for the Signal-to-Noise Ratio (SNR), Signal-to-Interference-Plus-Noise Ratio (SINR), multipath and optical power. Another approach to channel modelling is using a statistical or probabilistic model, such as the one proposed for this research which gives a statistical distribution of channel errors.

Modelling the errors on a channel using a single error probability is simple, yet it cannot describe more complex error distributions and patterns. The Fritchman model has multiple states and error probabilities. This means that the Fritchman model can potentially provide a better overall model for channel error distributions and patterns [4].

Channel modelling for VLC in general has not been studied considerably. The application of the Fritchman model in modelling a VLC channel is not evident in literature either. There have been several efforts to determine physical channel models where a signal approach has been taken. A statistical or probabilistic approach in determining channel error distributions have been applied in other communication fields. Below are details on existing work on statistical and signal approaches for VLC channel modelling.

---

[1]Adapted from [9]
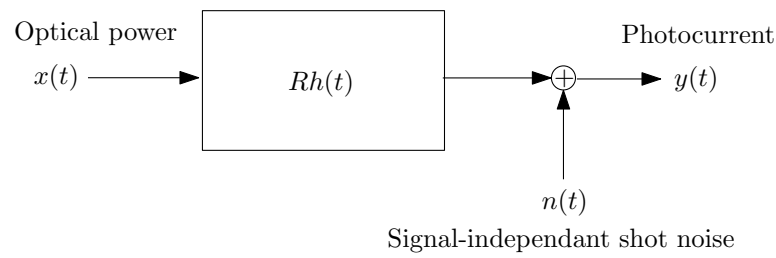
Figure 2.2: Baseband-equivalent optical link model [2]

2.3.1 General Transmission Link Model

The IM/DD approach that most VLC systems use is favourable because it reduces implementation complexity and costs of VLC systems. Let $x(t)$ denote the intensity of the LED and $y(t)$ denote the photocurrent of the receiving photodiode. As shown in Figure 2.2, the equivalent of the baseband signal for the optical link is given by [33]:

$$y(t) = x(t) \otimes Rh(t) + n(t) \tag{2.1}$$

where R is the responsivity of the photodiode, $h(t)$ is the baseband Channel Impulse Response (CIR), and $n(t)$ is Additive White Gaussian Noise (AWGN) and $\otimes$ denotes the convolution [33]. Receiver noise $n(t)$ is mainly as a result of ambient light. This includes natural light, such as sunlight, as well as artificial light from sources such as incandescent and fluorescent lamps. This can potentially degrade the performance of VLC. During the day, the noise would be dominated by sunlight.

2.3.2 Luminous Flux

A fundamental part of modelling a transmitting LED is understanding the radiometric and the photometric parameters. These parameters can then be used in either the spatial or spectral integrals to calculate the Luminous Flux, F_T, of the LED. This depends on which parameters are available.

---

[2]Adapted from [33]

Spectral Integral

This method uses the human eye's luminosity function, $V(\lambda)$, and the spectral power distribution, $S_T(\lambda)$, of an LED [33].

$$F_T = 683(\text{lumens/watt}) \int_{380nm}^{750nm} S_T(\lambda)V(\lambda)d\lambda \qquad (2.2)$$

The luminous efficiency of an LED in this case is the amount of electrical power required to produce a single lumen at 555 nm. This is the wavelength of light that the human eye is most sensitive to. It requires 1/683 watts to produce a single lumen at 555 nm.

Spatial Integral

Unlike the LED's luminosity function which measures the amount of light emitted, there is the luminous intensity, $g_t(\theta)$, which measures the LED's brightness in a certain direction in candelas. From the intensity distribution, the axial intensity, I_0, and the half-beam angle, θ_{max} are obtained. I_0 is the luminous intensity at $0°$ and θ_{max} is the angle where the light intensity is half I_0. Using the entire beam angle, θ_{max}, to calculate the θ_{max} [33]:

$$\Omega_{max} = 2\pi(1 - \cos\theta_{max}) \qquad (2.3)$$

Substituting this into Equation (2.4) below, and using the distribution of the normalised spatial luminous intensity, $g_t(\theta)$, the luminous flux can be determined [33].

$$F_T = \int_0^{\Omega_{max}} I_0 g_t(\theta)d\Omega \qquad (2.4)$$

$$F_T = I_0 \int_0^{\Omega_{max}} 2\pi g_t(\theta)\sin\theta d\theta \qquad (2.5)$$

2.3.3   Path Loss

The path loss, L_L, can be calculated using the luminous flux. It is the ratio of the luminous flux at the receiver, F_R, and the transmitter, F_T. The relative positions of

the transmitter and receiver need to be firstly specified, which are, their distance D, the incident angle α, the transmitter irradiation angle β, the receiver solid angle Ω_r and the receiver's area A_r. Then [33]:

$$A_r \cos \alpha = D^2 \Omega_r \tag{2.6}$$

The receiver flux is calculated as

$$F_R = I_0 g_t(\beta) \Omega_r \tag{2.7}$$

Using Equations (2.5), (2.6) and (2.7) yields [33]

$$L_L = \frac{F_R}{F_T} = \frac{g_t(\beta) A_r \cos \alpha}{D^2 \int_0^{\theta_{max}} 2\pi g_t(\theta) \sin \theta d\theta} \tag{2.8}$$

As most LEDs follow a Lambertian beam distribution, the spatial luminous intensity function is [33]

$$g_t(\theta) = \cos^m(\theta) \tag{2.9}$$

The value of m (Lambertial emission order) is dependant on the LED's semi-angle at half luminance $\Phi_{1/2}$ [33]

$$m = \frac{\ln(2)}{\ln(\cos \Phi_{1/2})} \tag{2.10}$$

Finally, doing a substitution of Equation (2.9) and θ_{max} into Equation (A)refeq:pos, it gives the LED's Lambertian path loss value [33]

$$L_L = \frac{m+1}{2\pi D^2} \cos \alpha \cos^m(\beta) \tag{2.11}$$

2.3.4 Received Power

Using the path loss, the received power can be calculated. Receiving photodetectors typically have an optical filter. The spectral response of the receiver's optical filter is denoted as $R_f \lambda$. Using this value, the LoS optical link is [33]

$$P_{RO} = \int_{\lambda_{rL}}^{\lambda_{rH}} S_R(\lambda) R_f(\lambda) d\lambda \qquad (2.12)$$

where $S_R(\lambda) = L_L S_T(\lambda)$. The λ_{rH} and λ_{rL} variables are the respective upper and lower wavelength cut-off values of the optical filter [1].

2.3.5 Multipath Propagation

It is typical to have more than one LED luminaire at the transmitter. This means that a receiver could receive multiple intensity modulated signals from the LEDs. The received optical power would then be calculated by a summation of all of the LoS links within the Field-of-View (FoV) [33]

$$P_R(\text{total}) = \sum_{i=0}^{N} P_R(i) \qquad (2.13)$$

where the number of LEDs is N and $P_R(i)$ is the received optical power from Equation (2.12).

Most indoor surfaces, such as walls and ceilings, have some reflectivity. These surfaces have a spectral reflectance, $\rho(\lambda)$, which is a function of wavelength. Due to these reflections, there are many different paths which the light travels before reaching the receiver. A Power Delay Profile (PDP) can be used to characterise this multipath propagation in which the received power distribution is represented as a function of the propagation delay. Taking this into consideration, the PDP can be modelled as multiple bounces from N LEDs at time t as [33]

$$h(t) = \sum_{n=1}^{N} \sum_{k=0}^{\infty} h^{(k)}(t; S_n) \qquad (2.14)$$

where k is the number of bounces and S_n is the spectral power distribution for the nth LED [34].

2.3.6   Noise and Interference

The most significant sources of noise and interference in the indoor VLC environment include (1) light from the sun through windows and doors, also known as ambient light, (2) photodetector shot noise which is a result of ambient light signals and (3) photodetector thermal noise. These produce a DC noise floor. Based on these effects, the Signal-to-Noise Ratio (SNR) is expressed as [33]:

$$\text{SNR} = \frac{P_S}{\sigma_{shot}^2 + \sigma_{thermal}^2 + P_B} \tag{2.15}$$

Considering the scenario where there is background noise and interference, the SINR is [33]

$$\text{SINR} = \frac{P_S}{\sigma_{shot}^2 + \sigma_{thermal}^2 + P_B + P_I} \tag{2.16}$$

where P_B and P_I are the background noise and interference powers respectively.

2.4   Indoor VLC Channel Modelling

This section includes a review of the some of the relevant works on indoor OWC channel modelling and characterisation.

The work by Komine and Nakagawa [15] was the first of its kind to do a fundamental analysis of OWC using LED lights. Simulations were done for a model room with LED lights to give distributions of received power, received power with reflection, and illuminance. These were based on several models described in the previous section. An AWGN channel with the shot noise being dominant was assumed. It was found that ISI degraded the performance significantly, and even more so with reflected ISI. The impact of data rate on the FoV was also studied. Overall, the work showed that indoor VLC using LEDs is feasible. Chun et al. [35] modelled a VLC channel that used OLEDs. The modelling was also for a model room, similar to that of Komine and Nakagawa.

Ray tracing is also a method of VLC channel modelling. Miramirkhani and Uysal [36] studied ray tracing of a simulated VLC environment from non-ideal sources under various conditions. These conditions included a variety of room dimensions, furniture placements and surface reflections. From the CIRs, the Root Mean Square (RMS) spread, DC gains, mean excess delay, coherence bandwidth and channel DC gain were obtained. These results showed specular components induced fluctuations in the CIR when compared to cases with diffuse reflections. The results also highlighted differences between Infra-Red (IR) and VLC channels where the DC gains and RMS delay spread are lower for IR channels. Similar work was done by Miramirkhani et al. [37], except in this work, the ray tracing was simulated in a scenario with a mobile user. The IEEE 802.15.7R1 task group has endorsed reference ray tracing channel models for VLC by Uysal et al. [38]. These models include four different, common scenarios which are a workplace, office room with secondary light, living room, and manufacturing cell. Each help with developing MIMO, OFDM and link layer techniques.

A comprehensive channel characterisation and modelling study was done by Sarbazi and Uysal [39]. In this paper, the channel modelling was done using ray tracing techniques in a simulated room environment. Practical issues such as mixing specular and diffuse reflections, wavelength dependency and higher order reflections were all incorporated into a simulation model. The ray tracing was performed in simulated room environments in cases where there were varying amounts of furniture. CIRs were shown to vary for different types of reflections. The paper further presents an investigation into the change on channel parameters with varying distance between the sender and receiver. Closed form expressions were obtained for the RMS delay spread and channel DC gain with respect to distance. The effects of sender and receiver specifications as well as environmental objects were also shown to have an effect on the CIR.

Similar work was done in [34] where the wavelength dependency and spectral reflectance of different reflectors were considered in the calculation of the power delay profile. Simulations were done in an empty room, multipath environment with plaster and plastic walls. The RMS delay spread and total received power from reflected paths were also shown to be smaller than that of IR, which is often assumed to have very similar characteristics to the visible light spectrum.

Chvojka et al. [40] studied the channel characteristics of indoor VLC in a dynamic environment. Both analytical and experimental results were obtained for a corridor, furnished room and an empty hall in cases with and without people present. For the

analytical aspect, received power and multipath channel models were considered. For the different environments with and without people present, the highest CDF of the received power differed up to 7% in the furnished room environment. The highest RMS delay spread of 6.5% was shown in the empty hall environment. Measurement results from an actual room produced optical power distributions for scenarios where up to three 1 m high objects were placed in the room. A standard deviation of up to 1.3 dB was shown when comparing the simulation with the actual measurements.

2.5 Outdoor VLC Channel Modelling

This section similarly reports relevant work in VLC channel modelling and characterisation for the outdoor environment, including V2V VLC.

Luo et al. [41] performed a fundamental analysis of a V2V VLC system that used LED-based headlamps. Mathematical models were derived for the car headlamp, road surface reflection and noise. These models were then used for BER analysis. It was shown that if the receiving photodiode is placed at a height between 0.2 m and 0.4 m, the distance between the transmitter and receiver can be up to 20 m and maintain a data rate of 20 Mbps. Improvements in these types of mathematical models were proposed by Cui et al. [42]. These models took into consideration the position and posture of the LEDs in V2V and V2I VLC channels.

Viriyasitavat et al. [43] derived a channel model for a real-life setting from empirical data using a Commercial-off-the-Shelf (COTS) scooter tail light. An SDR backend and a photodiode receiver were used as part of the experimental hardware. 4-PPM was chosen as the modulation scheme. Received power at the receiver was measured with a spectrum analyser around the carrier frequency. Their experimental results showed that the existing Lambertian optical channel model was unable to estimate the behaviour of the channel accurately enough. The authors thus proposed a new channel model that better predicts the behaviour of the channel. However, it is evident that the model that was developed may be specific to the type of tail light used. Experiments were conducted in both static and dynamic, real-life settings.

In a work by Cui et al. [44], COTS LED traffic lights were used as transmitters in a study of interference, artificial lighting and background solar radiation. Measurements for these were used in an analytical path model for the transmitters in an unobstructed LoS configuration. The model was validated using experimental results. Electrical power spectrum measurements were done at night for different artificial light sources.

These included a street light, neon sign board and large video LED screen. The measurements showed that the lower frequencies of the electrical power spectrum (up to 1 MHz) may produce a significant amount of interference in the channel.

Another model was developed by Wu and Tsai [45] using empirical data to model the link duration of V2V VLC scenarios. This was done using a video recorder that was mounted on a car and driven around urban and non-urban areas. Post-processing was done on the video recordings in order to identify the tail-lights of other vehicles on the road. Link durations for non-urban areas proved to be longer than in urban areas, and that single lane roads have longer link durations compared to two or three lane roads. Results showed that the link duration was in the order of seconds. It was found that the link duration could be modelled using a generalised Pareto distribution which can be used for VLC link duration analysis.

2.6   Baum-Welch Algorithm

The Baum-Welch algorithm was first described by Baum et al. [6]. It is an iterative technique used for finding the parameters of a Hidden Markov Model (HMM). This is done by using measured or simulated error sequences and initial values of the model parameters as the algorithm inputs. The Baum-Welch algorithm converges to a maximum likelihood estimator that maximises the model parameters based on the error sequences.

Some of the foremost applications of the Baum-Welch algorithm is in speech recognition [46, 47, 48] and cryptanalysis [49]. Erkurt and Proakis [50] used the Baum-Welch algorithm for joint data detection and channel estimation for channels that have rapid fading. Sivaprakasam and Shanmugan [51] used a modified Baum-Welch algorithm to estimate the parameters of Markov model from an observation sequence of a digital channel. Choi and Hwang [52] also used the Baum-Welch algorithm for audio-to-visual conversion based on an HMM inversion technique.

There have been some modifications of the Baum-Welch algorithm. Baggenstoss [53] made modifications for HMMs parameter estimation with multiple observation spaces. Turin and Sondhi [54] modified the Baum-Welch algorithm applied to digital channels to reduce computational requirements in cases where the observed error sequences have long stretches of observations which are identical.

2.7   HMM and Fritchman Model

In a recent work by Lui et al. [55], an HMM was used to characterise the non-linear effects in transmission of weakly illuminated LEDs. From the HMM, a Monte-Carlo method was used to determine what the achievable transmission rate is. The Viterbi algorithm was used in order to detect these weak signals under the HMM.

Fritchman [5] proposed the characterisation of channels using finite-state Markov chains in discrete-time. The Fritchman model has been used in the past as it is suitable for modelling burst error distributions [5]. It is also possible to estimate the model parameters conversely by measured or simulated burst error distributions. Fritchman derived both the error run and error-free run distributions. It is these distributions that can be applied to code evaluations.

Familua and Cheng [56] used the Fritchman model and Baum-Welch algorithm to model noise in a power line communication (PLC) band. The authors proposed a three state Fritchman model, with two good states and one bad state. Models were developed in both residential and laboratory environments for three different sources of noise in the channel; background noise, narrow band interference and impulse noise. These noise observations were gathered by experimental measurement. In order to obtain the error sequence, a noise threshold was set and any measured signal above the threshold was considered an error. It was found that the Baum-Welch algorithm needed to be executed at least 20 times before the model parameters were obtained within a sufficient level of accuracy. Familua et al. [57] also modelled a low complexity FSK-OOK integrated in-house PLC and VLC system using the Fritchman model. Another work by Ndjiongue et al. [58] also shows modelling of a hybrid PLC-VLC channel. Similar work in the field of PLC was done by Tina et al. [59] and Familua et al. [60].

Costamagna et al. [61] developed an indoor wireless channel model also using the Fritchman model and Baum-Welch algorithm in order to characterise the Digital Enhanced Cordless Telecommunications (DECT) technology at different interference levels and receiver speeds in an office environment. The authors reported that, in general, channels that are more bursty require a larger number of states in the model, which makes for a more simple model. Another finding was that if the analysis of the short-term behaviour of the channel is of interest, the model can remain simple.

Van Heerden and Ferreira [62] applied the Fritchman model using the Baum-Welch algorithm to model the error sequences of frequency hopped Very High Frequency

(VHF) digital channels, for both mobile and stationary scenarios. The mobile readings took place on an urban freeway. These error sequences were obtained from measurements on each of those two channels. Four-state Fritchman models were developed from the urban environment using FSK, DPSK, QPSK and 8-ary PSK modulation schemes. From curve fitting, it was found that five-state Fritchman models showed little difference in accuracy compared to the four-state model. The results were used to develop error correction techniques and it was found that, for the channels investigated, Reed-Solomon codes were the optimum types of codes. A similar work employing the same techniques was done by Swarts and Ferreira [63] in which they showed that certain observations were modelled better by the Fritchman model due to differences in receiver moving speed and the signalling interval. This was attributed to differences in Doppler rate.

Dobre et al. [64] provide another case where the VHF channel is modelled using the Fritchman model. However, in this case, models were derived for both urban and rural areas with the receiver travelling at different speeds using FSK and 8-PSK modulation for different tests. Modelling results showed that differences in model transition probabilities were dependant on the signalling method as well as the vehicle speed, which was attributed to the Doppler shift.

García-Frías and Crespo [65] used HMMs to characterise the burst errors in indoor Code-Division Multiple-Access (CDMA) radio links. The authors proposed a Hidden Markov Generative Model (HMGM) which is suitable for characterisation of the channels that have long error bursts. These models were also parametrised by the Baum-Welch algorithm. In addition to the HGM, a Fritchman model was also developed. Both of these models were based on the experimental error sequences from the radio links. The error-free run distribution, error cluster distribution and absolute value of the normalised covariance of the indoor readings for the HGM and the Fritchman model were compared. Results showed that the HGM were statistically close to the measured error sequences and showed a significant improvement over the Fritchman model. This improvement was mainly due to the high number of states the HGM consisted of, which means the model had higher complexity.

Another example of where the Fritchman model was applied to wireless links was in the work by Chouinard et al. [66]. The model was developed using error sequences from experiments involving a fixed transmitter and mobile receiver using a PSK modulation scheme in a medium-density urban environment. This model also consisted of a four-state Fritchman model. In this case, the model parameters were estimated using the gradient method. Error-free runs were also used in this case

to compare error sequences simulations with actual error sequences. The work also showed that for some of the experimental data, the Gilbert model proved sufficient to describe the channel.

Van Rooyen et al. [67] did a comparison of the Fritchman model and a Binary Symmetrical Channel (BSC) model that had the same error rates in a Direct-Sequence Spread-Spectrum Multiple-Access (DS/SSMA) system. This was done in scenarios with a varied number of users and processing gain. The comparisons using Error-Free Run Distribution (EFRD) plots showed that the Fritchman models were substantially different from the BSC and even displayed characteristics of a channel with memory. In this case, the Fritchman model was able to show how the errors on the channel occurred, unlike using a single BER value for a BSC to describe the errors. Another work by Van Rooyen and Ferreira [68] parametrised a Fritchman model for direct sequence spread spectrum under multi-user and multipath conditions. The parameters of each model also included SNR and processing gain. Models were derived for tests with a specific SNR value, within a certain SNR range.

Other works using the Fritchman model for modelling Rician fading channels [69], Rayleigh fading Global System for Mobile (GSM) communication channel [70], a simulated Longer Term Evolution (LTE) system [71] and digital magnetic tape recordings [72] are also worth noting.

2.8   VLC Channel Interference

Interference in the VLC channels presents a significant challenge to full realisation of the technology [1, 8]. This applies to both indoor and outdoor environments [7].

In an early work by Moreira et al. [73], artificial light interference from fluorescent and incandescent lights were characterised and modelled using experimental measurements in optical wireless channels. Measurements showed that the artificial light has the potential to produce a significant amount of interference in bands where transmission speeds are in the order of Mbps. It was found that fluorescent lights with their wider band have higher potential to degrade the optical channel. This highlighted the importance of considering the effects of artificial lights in an OWC system. A more recent work by Rahaim and Little [74] analysed the optical interference in VLC networks.

A highly relevant work by Kizilirmak and Kho [75] presents an interference mitigation

technique for OFDM based VLC. The authors highlight a probable use case of VLC where one luminary is transmitting data using OFDM, and the other is dimmed with PWM. This has potential in smart lighting applications where one LED is transmitting data and the other is not. This presents a unique challenge for the transmitting LED because now the channel has an interfering PWM signal. The authors suggest that the source of errors can be attributed to the periods where interfering PWM transitions take place. The PWM signal simply adds a DC offset to the received signal when the PWM transitions are not taking place.

2.9   Conclusion

The chapter began with an overview of VLC in which typical hardware, modulation techniques and applications were detailed. The IEEE standard for VLC was also presented which highlighted the frequency band used for outdoor VLC. A detailed review of current signal-level channel models used in VLC was also given. Literature on these signal-level models were presented. A large portion of the chapter showed how statistical channel models, namely HMM and Fritchman models, have been used in the past to provide high level, statistical models for wireless communication channels. Many of these works used the Baum-Welch algorithm for estimating the channel parameters. Finally, a review was given of literature on optical channel interference.

Chapter 3

Related Techniques

3.1   Introduction

This chapter presents details on the mathematical techniques used for the research to derive the channel models. This includes details on a generalised Markov model, leading to the Fritchman model. Details of each step of the Baum-Welch algorithm is also given. Finally, the evaluation criteria used for the channel models is presented.

3.2   Markov Models for Discrete Channels with Memory

Discrete channel models are different from waveform models in that they abstract out the waveform signal. A waveform signal consists of a sampled combination of the transmitted signal as well as disturbances such as noise and interference, whereas a discrete channel model is in terms of symbols only. Discrete channel models are favourable because they are computationally more efficient when compared to waveform channel models. With the physical aspects of the signal being abstracted out, the signal can then be characterised in terms of a smaller set of parameters. An important part of the modelling process is determining these parameters. This can be accomplished by physical measurements on the actual channel or by single waveform-level simulations.

For a channel that has memory, the discrete-time, finite-state Markov Model (MM) is most commonly used. The MM is favourable because it has been applied successfully to a number of different, significant communications problems. MMs can be used in

evaluating the channel capacity of a discrete channel, and for the designing of source encoders, interleavers and error control coding techniques [4].

For a discrete communication channel MM, at a given point in time, the channel can be in N number of states $S = S_1, S_2, S_3, ..., S_N$. As time progresses, the channel can transition between these states. This can be represented by the state transition matrix $\mathbf{A}$. The elements a_{ij} are defined as the probability of transitioning from state i at time t to a different state j at time $t+1$. It is represented by $a_{ij} = \Pr[S_{t+1} = j | S_t = i]$ where $i, j = 1, 2, 3, ..., N$. Thus [4],

$$\mathbf{A} = \begin{bmatrix} a_{11} & a_{12} & \cdots & a_{1i} & \cdots & a_{1N} \\ a_{21} & a_{22} & \cdots & a_{2i} & \cdots & a_{2N} \\ \vdots & \vdots & \ddots & \vdots & \ddots & \vdots \\ a_{N1} & a_{N2} & \cdots & a_{Ni} & \cdots & a_{NN} \end{bmatrix} \tag{3.1}$$

Within each state, there is probability that a transmission error will occur in the channel. For a binary symbol alphabet, the error symbols are denoted as $E = \{0, 1\}$ where a 0 denotes no error and a 1 denotes an error. Given that the model is in state i, there is a probability that the error symbol e_k will occur, which is denoted as $b_i(e_k) = \Pr[e_k | S_t = i]$. This is represented in the error generation matrix [4]:

$$\mathbf{B} = \begin{bmatrix} b_{11} & b_{12} & \cdots & b_{1i} & \cdots & b_{1N} \\ b_{21} & b_{22} & \cdots & b_{2i} & \cdots & b_{2N} \end{bmatrix} \tag{3.2}$$

The final parameter is the initial state probability. This describes the probability of being in any of the N states at $t = 1$, or at the beginning of the observation. It is denoted as $\Pi = \Pr[S_1 = i]$ where $i = 1, 2, 3, ..., N$, or [4]

$$\Pi = \begin{bmatrix} \pi_1 & \pi_2 & \pi_3 & \cdots & \pi_N \end{bmatrix} \tag{3.3}$$

3.3 Fritchman Model

For the case of binary channels, the Fritchman model framework partitions the channel state space into good and bad states. Fritchamn defined k good states representing
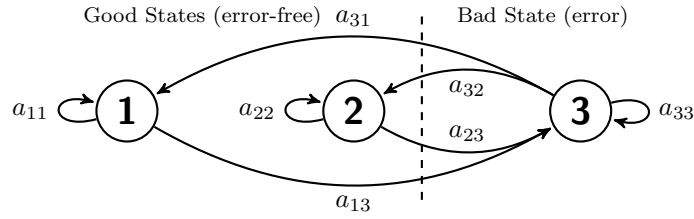
Figure 3.1: Fritchman model with two good states and one bad state.

error-free transmissions and $N - k$ bad states representing a transmission where an error always occurs.

Three-state Fritchman models were chosen in order to limit the complexity of using a higher number of states. Figure 3.1 shows a three state Fritchman model. Transitions only occur between good and bad states, and never from a good state to another good state. This is because the transitions between good states are indistinguishable as the output is always error-free. In other words, the transition is not observable. The resultant **A** matrix would thus be [4]

$$\mathbf{A} = \begin{bmatrix} a_{11} & 0 & a_{13} \\ 0 & a_{22} & a_{23} \\ a_{31} & a_{32} & a_{33} \end{bmatrix} \tag{3.4}$$

Due to the fact that errors are produced only when the channel is in a bad state, the **B** matrix simply consists of 1's and 0's. The first two columns of the matrix represent error-free states and the last column represents the error state [4]

$$\mathbf{B} = \begin{bmatrix} 1 & 1 & 0 \\ 0 & 0 & 1 \end{bmatrix} \tag{3.5}$$

The final parameter for a three-state model is the initial state probability [4]

$$\mathbf{\Pi} = \begin{bmatrix} \pi_1 & \pi_2 & \pi_3 \end{bmatrix} \tag{3.6}$$

In this particular case, the model can be said to be an SHMM. This is because when an error is observed, it is due to the channel being in only a single bad state. If no error has occurred, it is difficult to know which one of the many good states the channel is in. It is for this reason that knowledge of the channel states is not completely hidden.

The Gilbert-Elliot (GE) model is a two-state MM with only one good state and one bad state [76]. Even though this model is simple, it is not flexible enough to be useful in modelling vast array of channels. It is possible that the model would not be able to account for more complex error distributions [5].

3.4   Baum-Welch Algorithm

The Baum-Welch algorithm is a robust method for fitting an MM. Using this algorithm, the parameters for the channel model [4],

$$\Gamma = (\mathbf{A}, \mathbf{B}, \mathbf{\Pi}) \tag{3.7}$$

can be estimated. This is an iterative algorithm that uses either a measured or simulated error sequence [4],

$$\overline{O} = \{O_1, O_2, ..., O_t, ..., O_T\} \tag{3.8}$$

to converge to the maximum likelihood estimator for the model parameters that maximises $\Pr(\overline{O}|\Gamma)$. The number of iterations depends on the desired level of accuracy for the model [6]. Included below is an overview of the steps of the Baum-Welch algorithm [4].

Step 1: Assume an initial model with some values for $\Gamma = (\mathbf{A}, \mathbf{B}, \mathbf{\Pi})$.

Step 2: Using the model $\Gamma = (\mathbf{A}, \mathbf{B}, \mathbf{\Pi})$, compute the *forward variables* [4]

$$\alpha_t = \Pr[O_1, O_2, ..., O_t, s_t = i|\Gamma] \tag{3.9}$$

and the *backward variables* [4]

$$\beta_t = \Pr[O_{t+1}, O_{t+2}, ..., O_T|s_t = i, \Gamma] \tag{3.10}$$

Forward variables Calculation of the forward variables involves the following steps [4]:

Initialisation:

$$\alpha_1(i) = \pi_i b_i(O_1), i = 1, 2, ..., N \tag{3.11}$$

Induction:

$$\alpha_{t+1}(j) = \left[\sum_{i=1}^{N} \alpha_t(i) a_{ij} \right] b_j(O_{t+i}), 1 \le t \le T - 1, 1 \le j \le N \tag{3.12}$$

Termination:

$$\Pr[\overline{O}|\Gamma] = \sum_{i=1}^{N} \alpha_T(i)\beta_T(i) \tag{3.13}$$

Backward variables Calculation of the backward variables involves the following steps [4]:

Initialisation:

$$\beta_T(i) = 1, i = 1, 2, ..., N \tag{3.14}$$

Induction:

$$\beta_t(i) = \sum_{i=1}^{N} \beta_{t+1}(j) b_j(O_{t+1}) a_{ij}, 1 \le t \le T - 1, 1 \le j \le N \tag{3.15}$$

Step 3: Using the forward variables and backward variables, the next step is to compute the expected frequencies, $\zeta_t(i, j)$ and $\gamma_t(i)$. $\zeta_t(i, j)$ represents the expected number of transitions from state i to j. It is computed according to [4]

$$\zeta_t(i, j) = \Pr[s_t = i, s_{t+1} = j|\overline{O}, \Gamma] = \frac{\alpha_t(i) a_{ij} b_j(O_{t+1}) \beta_{t+1}(j)}{\Pr[\overline{O}|\Gamma]} \tag{3.16}$$

$\gamma_t(i)$ represents the expected number of transitions from i. It is computed according to [4]

$$\gamma_t(i) = \Pr[s_t = i|\overline{O}, \Gamma] = \frac{\alpha_t(i)\beta_t(i)}{\Pr[\overline{O}|\Gamma]} \tag{3.17}$$

Step 4: Using the expected frequencies, the new state transition probabilities $\hat{a}_{ij}$ are calculated by [4]

$$\hat{a}_{ij} = \frac{\text{expected number of transitions from } i \text{ to } j}{\text{expected number of transitions from } i} = \frac{\sum_{t=1}^{T-1} \zeta_t(i,j)}{\sum_{t=1}^{T-1} \gamma_t(i)} \tag{3.18}$$

Then, $\hat{b}_j(e_k)$ is computed [4]

$$\hat{b}_j(e_k) = \frac{\text{expected number of times } e_k \text{ is emitted from state } j}{\text{expected number of visits to state } j} = \frac{\sum_{t=1|O_t=e_k}^{T} \gamma_t(j)}{\sum_{t=1}^{T} \gamma_t(j)} \tag{3.19}$$

Step 5: Repeat steps 2 - 4 using the newly computed model parameters $\hat{\Gamma} = (\hat{\mathbf{A}}, \hat{\mathbf{B}}, \hat{\mathbf{\Pi}})$ until the desired level of convergence has been reached.

3.5   Evaluation Criteria of Modelling

3.5.1   Log-likelihood

One way to determine the convergence of the Baum-Welch algorithm is to run the algorithm iteratively until successive values $Pr[\overline{O}|\Gamma]$ differ by very little. This is because the Baum-Welch algorithm is guaranteed to converge to a maximum likelihood. The log-likelihood can be used for not only determining convergence, but also for evaluating how well the model represents the channel. It is evaluated by the following in terms of a scaling constant C_t [4]

$$\Pr[\overline{O}|\Gamma] = \prod_{t=1}^{T} C_t \tag{3.20}$$

$$\log_{10}\Pr[\overline{O}|\Gamma] = \sum_{t=1}^{T} \log_{10}C_t \tag{3.21}$$

3.5.2   Error-free Run Distribution Plot

Another way to evaluate the model is by using the EFRDs, $\Pr(0^m|1)$, which is the probability of transitioning to m or more consecutive error-free states following the occurrence of an error. The distributions of $\Pr(0^m|1)$ for both the original measured data and the data generated from the channel model approximated by the Baum-Welch algorithm can be plotted and compared [4]. Furthermore, the deviations in these two plots can be evaluated by determining the mean squared error. The chi-squared test can also be used to determine if there are significant differences between the approximated model frequencies and the original data frequencies.

3.6   Conclusion

This chapter presented the techniques that were used to derive and analyse the channel models. The Fritchman model was presented in detail, showing how it can be used for modelling a channel from a discrete error sequence. The Baum-Welch algorithm used to iteratively estimate the model parameters was also presented in detail. Log-likelihood plots are used to determine the convergence of the model parameters. Models can be analysed by using the EFRD in order to see the error patterns and distributions.

Chapter 4

Indoor Modelling

4.1 Introduction

The first part of the research is focused on the indoor environment where interference from nearby light and LEDs are present. This chapter explains each of the interference and noise scenarios, the hardware that was designed and used for conducting the experiments, the experimental procedure and and, finally, a discussion of the results.

4.2 Model Scenarios

Models were developed for three different indoor channels with different noise and interference present. The interference in these cases would be from a nearby smart lighting LED. The three different cases are:

   I Background noise from sunlight passing through windows and from fluorescent indoor lighting.

  II The same background noise as case I as well as an interfering PWM modulated LED. This case includes three sub-cases for different PWM dimming levels, namely 25%, 50% and 75% duty cycles.

 III The same background noise as case I as well as an interfering OOK modulated LED transmitting pseudo-random binary data.

Experiments for each of these cases took place in a lab environment that includes a number of windows and fluorescent lights.

4.3   System Description

4.3.1   Hardware

Figures 4.1 and 4.2 shows a photograph of the experimental setup with the transmitter and receiver boxes. Figure 4.3 shows a detailed block diagram of the system, which includes transmitter, interferer and receiver modules.

The transmitter's Arduino Nano outputs an OOK signal to the MOSFET circuit which then drives the white LED. The OOK signal is received at the photodiode and then converted from a current signal to a voltage signal by means of a Transimpedance Amplifier (TIA). The Analog-to-Digital Converter (ADC) at the receiver's Nano samples the signal and determines whether the received bit is a 1 or a 0 based on a decision threshold. Communication between the transmitter and receiver is synchronised by a clock line. In a practical VLC communication system, a clock line would not be practical. However, seeing as this work is on channel characterisation, a clock line is acceptable. This clock line is necessary to reduce the likelihood of having any synchronisation errors. Thus, almost all of the errors should come as a result of the channel. The interferer transmits a signal in the same manner as the transmitter. The transmitter module controls when the interferer should be activated as part of the experimental procedure.
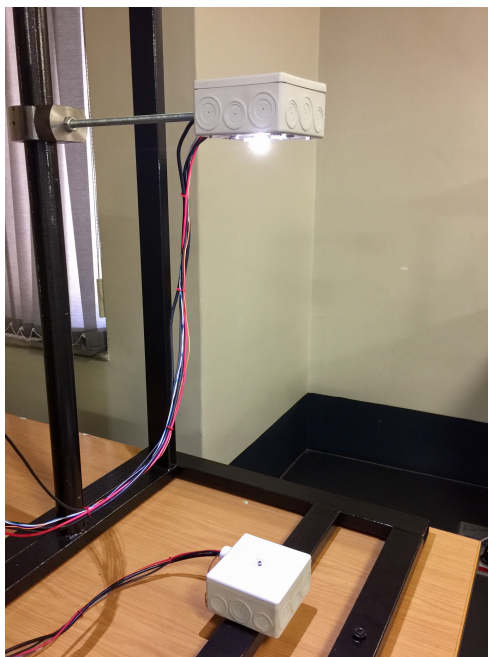

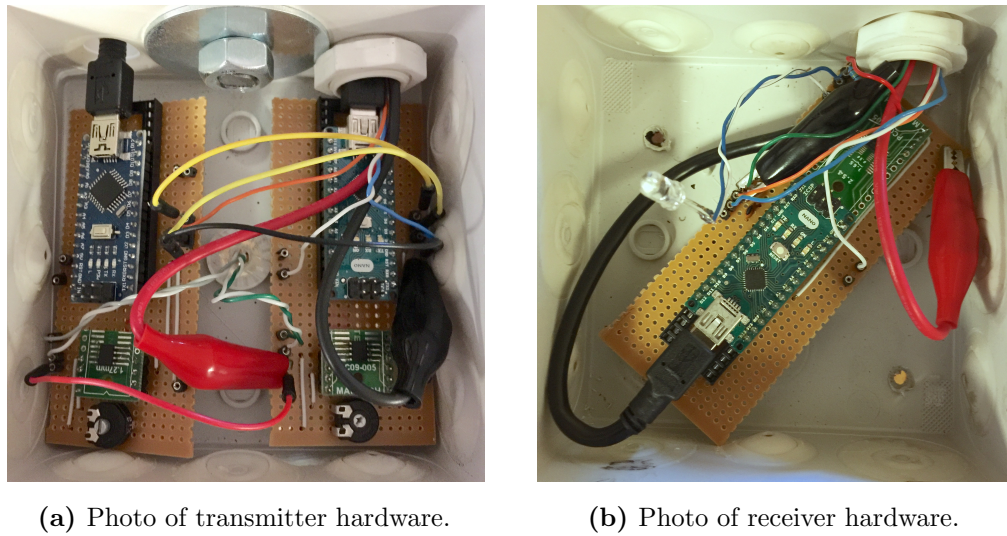**Figure 4.1:** VLC indoor transmitter and receiver with stand.

(a) Photo of transmitter hardware.   **(b)** Photo of receiver hardware.
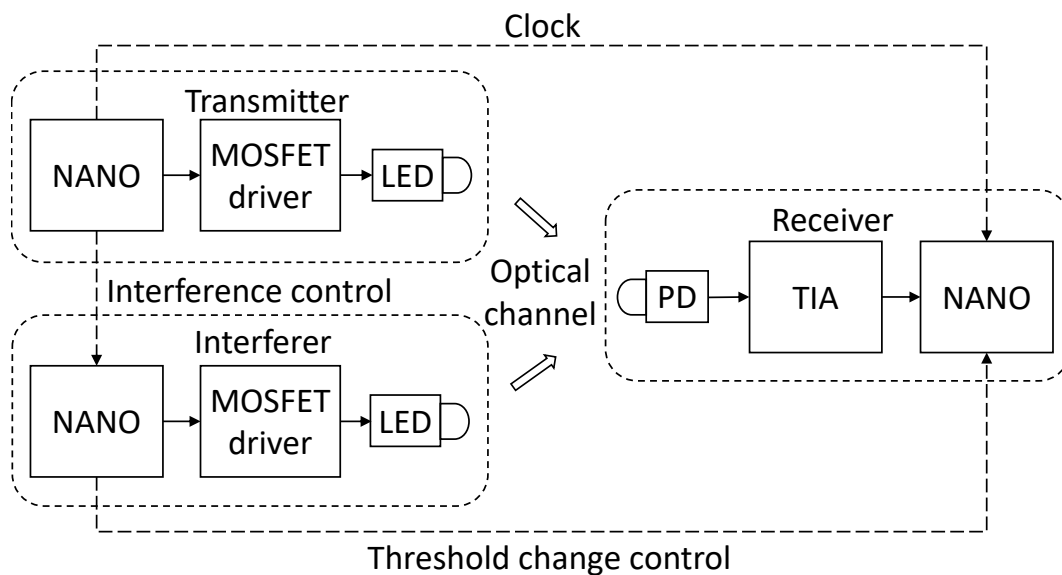
Figure 4.2: VLC system hardware.

Figure 4.3: Block diagram of VLC system used to obtain error sequences.

4.3.2 Decision Threshold

At the receiver, the ADC threshold value is different for each experimental case. For case I, there is a single threshold value. Figure 4.4 shows an example of the two thresholds used for case II at the receiver. V_{th1} is used when the interfering PWM signal is on and V_{th2} for when it is off. This is because when the PWM signal is on, it simply adds a DC offset to the received signal. Note that the PWM signal has an additional DC offset as a result of background noise. The interferer informs the receiver when it needs to change its threshold value while a transmission is taking
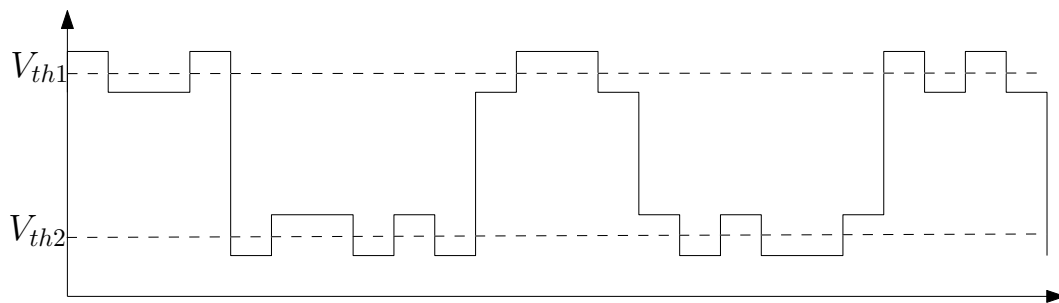
Figure 4.4: Voltage waveform with bit sequence, PWM interference, and background noise DC offset measured at the receiver, showing two decision thresholds.

place. The justification for this approach is that a PWM signal is deterministic and it is possible to change threshold without a connection between the interferer and receiver. However, the implementation of this is beyond the scope of this research. These approaches result in an optimal threshold detection for cases I and II.

Threshold values are determined at the beginning of each transmission by sending pilot bit sequences. The pilot bits are sent once for case I. For case II, the pilot bits are sent twice; once for when the PWM signal is on, and again for when the PWM signal is off. The same pilot bits are also sent at the end of a transmission.

The random binary signal transmitted by the interferer in case III is non-deterministic. In practise, this makes it more difficult to determine when to change the decision threshold. As such, a decision threshold is taken by getting the average ADC values of the sampled random signal, and using this as the decision threshold. This results in a sub-optimal decision threshold.

4.4   Experimental Procedure

For each case, 100,000 pseudo-random bits were transmitted at a rate of 6.25 kbps in 10,000 bit chunks. The interfering PWM signal has a frequency of 600 Hz with duty cycle values as per the case II description (see Section 4.2). Transmissions were run for all three of these case II duty cycles. Transmission distance was fixed at 1m. In order to get a variety of modelling results, a number of transmissions took place for each case within a range of SNR in case I, or SINR in cases II and III. This was done by varying the optical power of the transmitter. Presently, there is no standard set for the maximum amount of optical power allowed to prevent interference on a nearby transmitting LED. The SNR and SINR range was chosen based on the number of errors in the error sequence, which was between approximately 1% and 10%. The

received binary sequence was compared with the known transmitted sequence to obtain an error sequence. A 1 in the error sequence denotes an error and a 0 denotes no error. This was then used as the input to the Baum-Welch algorithm. A detailed description of how SNR was calculated is included in Appendix A.

Along with the error sequences collected for each case, initial values for the model parameters were used as the input for the Baum-Welch algorithm, which include:

$$\mathbf{A} = \begin{bmatrix} 0.9 & 0 & 0.1 \\ 0 & 0.8 & 0.2 \\ 0.1 & 0.7 & 0.2 \end{bmatrix} \tag{4.1}$$

$$\mathbf{B} = \begin{bmatrix} 1 & 1 & 0 \\ 0 & 0 & 1 \end{bmatrix} \tag{4.2}$$

$$\mathbf{\Pi} = \begin{bmatrix} 0.4 & 0.4 & 0.2 \end{bmatrix} \tag{4.3}$$

4.5   Results and Discussion

4.5.1   Model Derivation and Comparison

The Baum-Welch algorithm was used to generate three-state Fritchman models. Increasing the number of states of the model yielded similar results for a model with only three states. This means that a three-state model is the minimum number of states needed to describe the channel in these particular scenarios in terms of a Fritchman model.

The resultant state transition probabilities of the models were used to generate new error sequences of 100,000 bits for the different channels at each SNR/SINR. In order to determine how well the models describe the channel, a comparison is made between a single BER value and the Fritchman model with its multiple states. Independent and Identically Distributed (IID) error sequences were generated using each sequence error probability, P_e, obtained from the experimental error sequence. The measured, modelled and IID error sequences were then compared using EFRD plots, or $\Pr(0^m|1)$. The EFRD from the measured sequence is compared to the

modelled and IID EFRD using the chi-squared (χ^2) test and Mean Squared Error (MSE) to determine goodness of fit.

Only models for cases I and II are presented. Models for case III are not presented because of the high number of errors (24.97%) in the error sequences. This was still the case even at a higher transmitter SINR. Channels with such high error probabilities would not be practical even when employing existing error control techniques. As such, a more robust method is required for threshold change and detection for case III in order to reduce the number of decision errors and develop practical channel models.

4.5.2   Case I

Table 4.1 shows the modelling results for case I along with comparisons of the models and IID χ^2 and MSE values. Each of the models for this case have lower MSE and χ^2 values. This indicates that the Fritchman model provides a more accurate way to model errors in a VLC channel with background noise, compared to a single BER value. Figure 4.5 shows one of the EFRD comparisons where the model follows the distribution of the measured sequence.
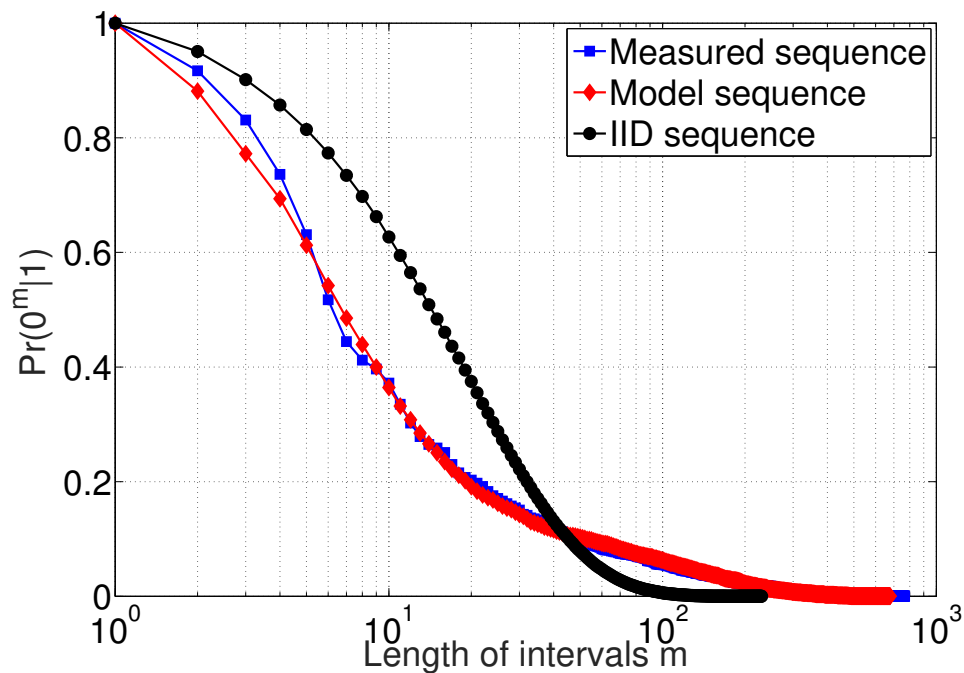

Figure 4.5: Channel with background noise from indoor lighting and windows at 4.73 dB SNR case I.

Table 4.1: Modelling Results for case I

SNR (dB)	P_e	Transition probabilities							MSE		χ^2	
		a_{11}	a_{13}	a_{22}	a_{23}	a_{31}	a_{32}	a_{33}	IID	Model	IID	Model
7.68	0.0067	0.9960	0.0040	0.9724	0.0276	0.5338	0.4320	0.0342	0.00283	0.00087	22.67724	8.76799
6.95	0.0238	0.9916	0.0084	0.9181	0.0819	0.2843	0.6067	0.1090	0.00424	0.00023	13.70263	0.72130
6.66	0.0502	0.9895	0.0105	0.8614	0.1386	0.1481	0.6712	0.1807	0.00576	0.00007	9.33804	0.12776
6.44	0.0363	0.9848	0.0152	0.8862	0.1138	0.3317	0.5483	0.1200	0.00270	0.00011	6.80294	0.37627
5.91	0.0449	0.9700	0.0300	0.9196	0.0804	0.4766	0.4321	0.0913	0.00040	0.00017	0.82839	0.20040
5.60	0.0480	0.9729	0.0271	0.8293	0.1707	0.4832	0.3926	0.1242	0.00165	0.00010	2.67459	0.12581
5.48	0.0840	0.9556	0.0444	0.8703	0.1297	0.3005	0.5473	0.1522	0.00056	0.00012	0.78514	0.10873
4.73	0.0905	0.9426	0.0574	0.8970	0.1030	0.2366	0.6135	0.1499	0.00037	0.00023	0.32733	0.18721
4.50	0.1039	0.9226	0.0774	0.8918	0.1082	0.1861	0.6724	0.1415	0.00020	0.00014	0.11204	0.06155
4.28	0.1281	0.9345	0.0655	0.8373	0.1627	0.2078	0.5917	0.2005	0.00041	0.00013	0.42408	0.30211

4.5.3   Case II

Tables 4.2, 4.3 and 4.4 show the case II modelling results for the 25%, 50% and 75% duty cycles respectively. The first half of the tables show that the models generated for case II have $a_{33} = 0$. This represents the probability of having two or more consecutive errors in the error sequence, forming error clusters. This means there are no error clusters. The χ^2 and MSE values show that the models do not always provide a better fit compared to the IID sequences in tests for case II. Figures 4.6, 4.7, and 4.8 show an EFRD from case II tests with similar SINR. The error sequence produced by the model is unable to follow the measured error sequence with significant improvement compared to the IID error sequence. It is evident that Fritchman models are better suited to channels that have error clusters. It is possible that a two-state GE model which formed the basis for the Fritchman model may have been sufficient to model these channels.

At higher SINR tests, the majority of errors appear to be caused by the interfering PWM signal. Between about 5 dB and -10 dB, the tests show P_e values that are consistently around 0.05. This is also around the region where $a_{33} = 0$. Thus, errors caused within this region are almost exclusively as a results of the interfering PWM signal. As the SINR decreases, errors are introduced from background noise as well,
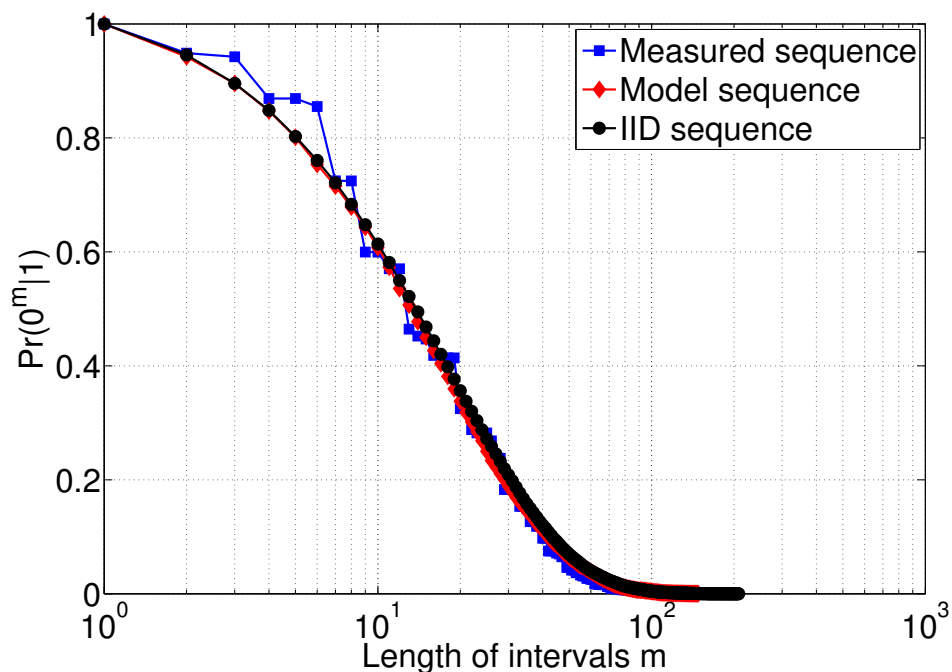

Figure 4.6: Channel with background noise and 25% duty cycle modulated LED interference at -9.55 dB SINR.
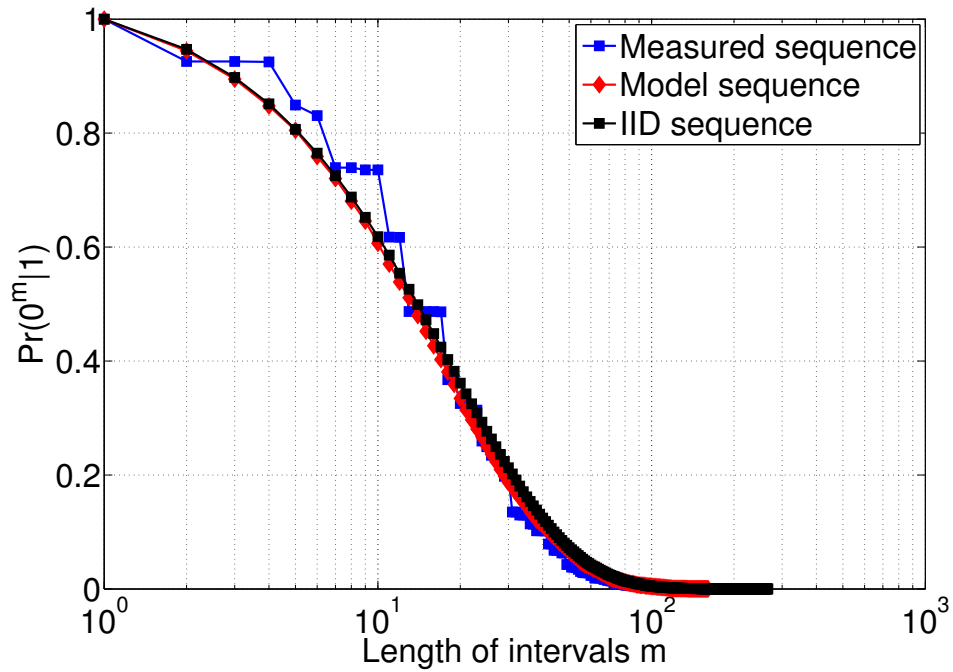
which increases the P_e and gives $a_{33} > 0$.

Figure 4.7: Channel with background noise and 50% duty cycle modulated LED interference at -8.55 dB SINR.
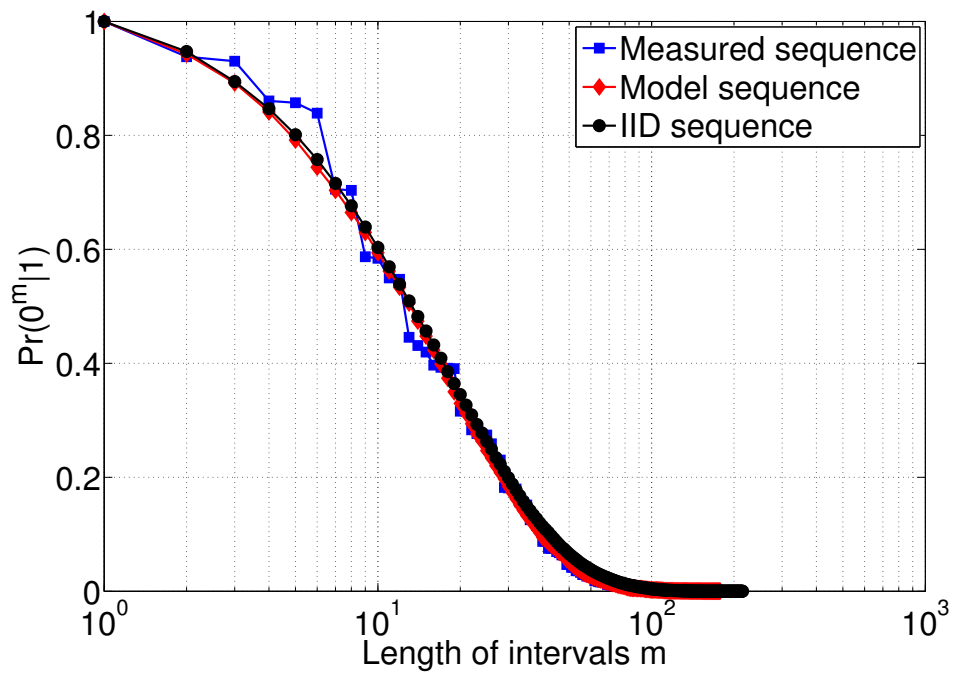

Figure 4.8: Channel with background noise and 75% duty cycle modulated LED interference at -10.68 dB SINR.

Table 4.2: Modelling Results for case II - 25% Duty Cycle Interference

| SINR (dB) | P_e | Transition probabilities | | | | | | | | | | MSE | | χ^2 | |
		a_{11}	a_{13}	a_{22}	a_{23}	a_{31}	a_{32}	a_{33}	IID	Model	IID	Model
5.57	0.0495	0.9481	0.0519	0.9477	0.0523	0.4014	0.5986	0.0000	4.24E-04	4.58E-04	0.9953	0.4541
-1.02	0.0501	0.9480	0.0520	0.9467	0.0533	0.3931	0.6069	0.0000	3.64E-04	3.35E-04	0.6167	0.3674
-2.04	0.0494	0.9486	0.0514	0.9476	0.0524	0.4015	0.5985	0.0000	3.68E-04	3.20E-04	0.7938	0.2031
-5.35	0.0512	0.9478	0.0522	0.9448	0.0552	0.3863	0.6137	0.0000	2.65E-04	2.21E-04	0.5570	0.2362
-9.55	0.0527	0.9451	0.0549	0.9439	0.0561	0.3724	0.6276	0.0000	3.29E-04	2.80E-04	0.7966	0.4347
-13.84	0.0523	0.9466	0.0534	0.9437	0.0563	0.3781	0.6215	0.0004	3.50E-04	3.65E-04	0.5347	0.3648
-16.33	0.1012	0.9142	0.0858	0.8945	0.1055	0.1800	0.7154	0.1046	7.69E-05	9.83E-05	0.0291	0.0427
-16.92	0.1056	0.9152	0.0848	0.8888	0.1112	0.1723	0.7159	0.1118	7.12E-05	6.33E-05	0.0254	0.0352
-18.71	0.0739	0.9351	0.0649	0.9201	0.0799	0.2584	0.6836	0.0581	1.59E-04	1.31E-04	0.0556	0.0459
-19.24	0.0861	0.9308	0.0692	0.9062	0.0938	0.2215	0.6951	0.0834	1.01E-04	9.41E-05	0.0385	0.0458

Table 4.3: Modelling Results for case II - 50% Duty Cycle Interference

SINR (dB)	P_e	Transition probabilities							MSE		χ^2	
		a_{11}	a_{13}	a_{22}	a_{23}	a_{31}	a_{32}	a_{33}	IID	Model	IID	Model
6.37	0.0486	0.9491	0.0509	0.9487	0.0513	0.3943	0.6057	0.0000	6.38E-04	6.01E-04	0.8494	0.4041
-0.58	0.0513	0.9461	0.0539	0.9458	0.0542	0.3744	0.6256	0.0000	6.74E-04	7.24E-04	1.0036	0.6290
-2.70	0.0575	0.9421	0.0579	0.9397	0.0603	0.3327	0.6426	0.0247	2.77E-04	2.26E-04	0.3368	0.1879
-6.20	0.0511	0.9466	0.0534	0.9459	0.0541	0.3754	0.6246	0.0000	6.01E-04	5.33E-04	0.7357	0.2321
-8.55	0.0518	0.9456	0.0544	0.9452	0.0548	0.3684	0.6316	0.0000	6.04E-04	5.45E-04	0.9099	0.4766
-12.03	0.0582	0.9404	0.0596	0.9388	0.0612	0.3291	0.6523	0.0186	3.09E-04	3.19E-04	0.4044	0.2140
-14.10	0.0586	0.9397	0.0603	0.9381	0.0619	0.3218	0.6641	0.0142	3.65E-04	3.62E-04	0.4813	0.2922
-14.64	0.0707	0.9295	0.0705	0.9263	0.0737	0.2658	0.6908	0.0434	1.77E-04	1.37E-04	0.1761	0.0717
-15.01	0.0912	0.9141	0.0859	0.9063	0.0937	0.1993	0.7163	0.0844	7.81E-05	7.53E-05	0.0484	0.0238
-16.32	0.0900	0.9168	0.0832	0.9067	0.0933	0.2022	0.7167	0.0811	6.82E-05	7.34E-05	0.0391	0.0528

Table 4.4: Modelling Results for case II - 75% Duty Cycle Interference

SINR (dB)	P_e	Transition probabilities							MSE		χ^2	
		a_{11}	a_{13}	a_{22}	a_{23}	a_{31}	a_{32}	a_{33}	IID	Model	IID	Model
5.47	0.0496	0.9485	0.0515	0.9473	0.0527	0.3962	0.6038	0.0000	3.31E-04	3.19E-04	0.6539	0.2470
1.25	0.0495	0.9485	0.0515	0.9475	0.0525	0.3956	0.6044	0.0000	3.55E-04	3.44E-04	0.7741	0.7049
-2.58	0.0514	0.9464	0.0536	0.9454	0.0546	0.3885	0.6115	0.0000	4.26E-04	4.79E-04	0.9859	0.6809
-6.05	0.0526	0.9451	0.0549	0.9441	0.0559	0.3762	0.6231	0.0008	3.44E-04	2.99E-04	0.9822	0.5474
-10.68	0.0542	0.9445	0.0555	0.9420	0.0580	0.3654	0.6305	0.0041	3.22E-04	2.63E-04	0.5839	0.1270
-12.20	0.0654	0.9378	0.0622	0.9299	0.0701	0.3013	0.6630	0.0357	1.85E-04	1.55E-04	0.2404	0.0768
-14.08	0.0650	0.9418	0.0582	0.9290	0.0710	0.3050	0.6490	0.0460	1.23E-04	1.07E-04	0.1063	0.1003
-15.65	0.0772	0.9392	0.0608	0.9123	0.0877	0.2534	0.6825	0.0641	1.18E-04	1.12E-04	0.0638	0.0861
-16.31	0.0824	0.9312	0.0688	0.9093	0.0907	0.2330	0.7021	0.0649	1.15E-04	9.56E-05	0.0455	0.0359
-18.80	0.1013	0.9204	0.0796	0.8909	0.1091	0.1844	0.7155	0.1001	5.63E-05	4.28E-05	0.0284	0.0631

The SINR values that were calculated and included as part of the results for case II are lower than expected. This is as a result of limitations in the SINR measurements. SINR and SNR values were calculated using variance from ADC readings. Inaccuracies in the ADC readings led to variance values for the noise term being much higher than anticipated. Figure 4.9 shows some of the ADC samples from case II. These specific samples were supposed to be grouped into readings of the background noise only. However, because the grouping had to take place in the presence of the interfering PWM signal, some samples that were supposed to be put into the interference group were put into the noise group. These are evidenced by the spikes in ADC samples in Figure 4.9. This invariably led to a higher denominator term, thus, reducing the SINR values. See Appendix A for more details on the SINR calculation.

4.5.4   Log-likelihood

For the generation of the models, the Baum-Welch algorithm was run 20 times. In order to test for the algorithm convergence, the log-likelihood ratios were plotted for cases I and II. The log-likelihood plots for four models are shown in Figure 4.10 for 10 iterations. Each of algorithms converged by the third iteration. The log-likelihoods for case II are similar, with the case I having a greater log-likelihood.
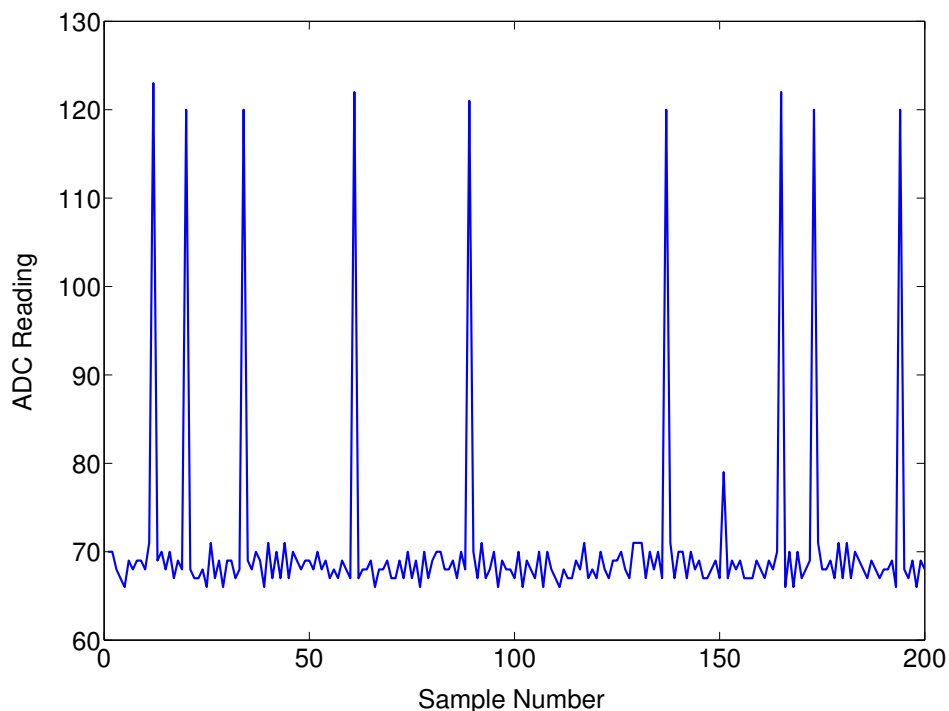

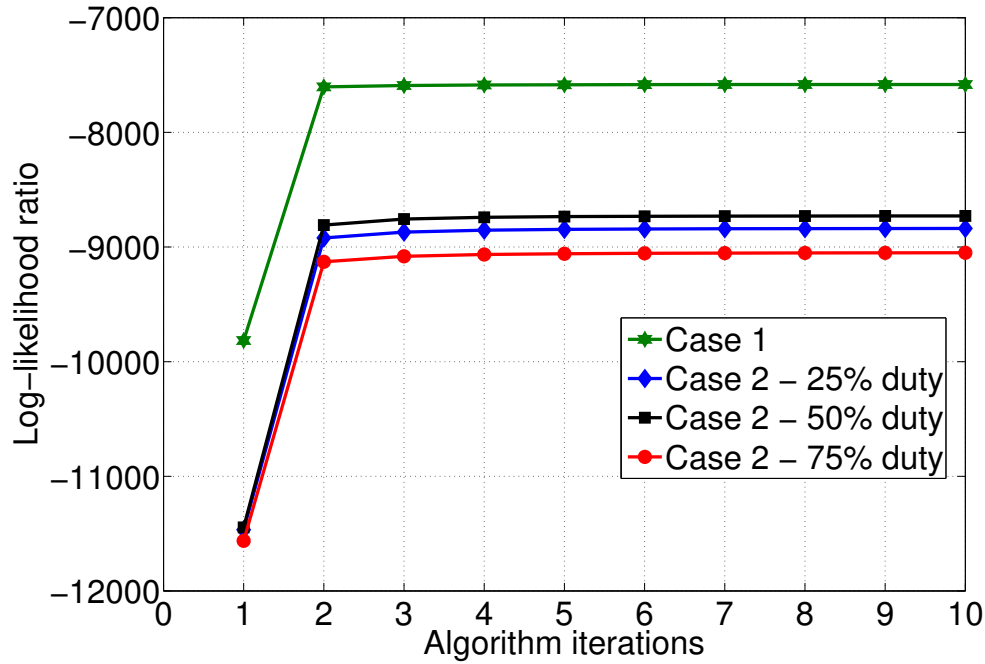**Figure 4.9:** Samples of ADC readings used for SINR calculations.

Figure 4.10: Log-likelihoods for 10 iterations of the Baum-Welch algorithm, cases I and II.

4.5.5   Discussion

The SINR values are significantly different for case II compared to tests with similar P_e values from case I. This is due to the dominance of the interfering PWM signal which adds a P_e increase of about 0.05. The errors from interference are also periodic in nature. This is due to the periodic interfering PWM signal. However, the periodic errors are not the same for different interference duty cycles. Figure 4.11 shows the EFRD for the measured sequences for tests from each of the three duty cycles. The 25% and 75% duty cycle interference EFRD show very similar distributions. This is because the signals are 180° out of phase. Upon closer observation, Figure 4.11 also shows evidence that the PWM transitions are also the source of errors, even with the optimal threshold detection. The gaps between these errors are dependant upon the gaps of the duty cycles. The PWM frequency is an order of magnitude higher than the transmission frequency. Thus, for a 50% duty cycle interference, there is a higher probability of errors every 10 bits. On the other hand, for 25% and 75% there is a similar error probability, except it is every 8 bits.
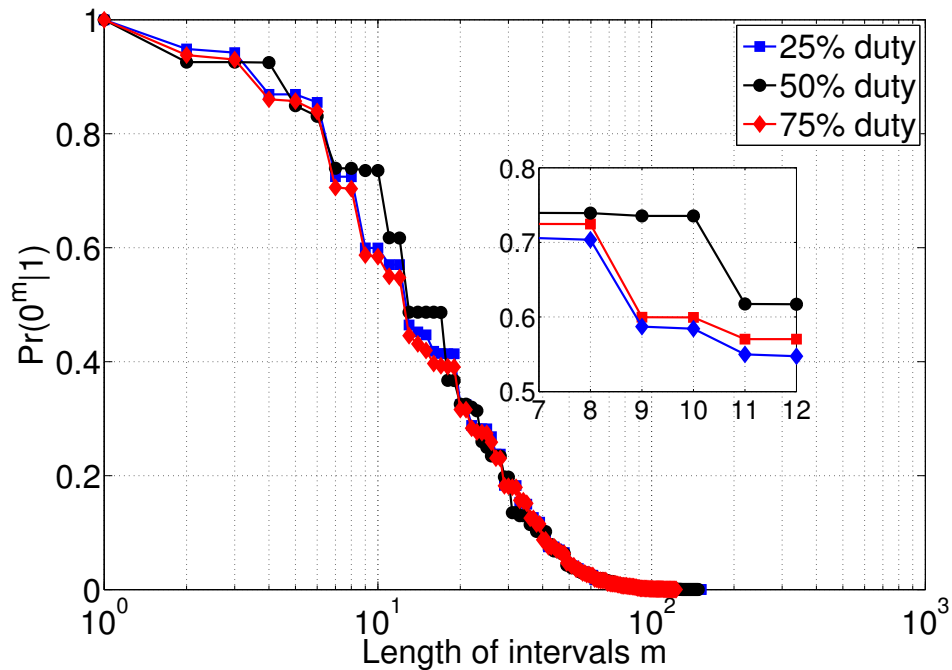
Figure 4.11: Comparison of EFRD from the different PWM interference scenarios.

4.5.6   Conclusion

Models for case I which included background nosie only were all able to provide good approximations of the channels. However, models for case II did not consistently provide good approximations of the channels. This was because of the dominant PWM interference which resulted in periodic errors, which led to few error clusters. The EFRD plots did provide some insight into the error patterns of interfering PWM signals. The 25% and 75% shows similarities in error distributions. These results can possibly help in the design of error control codes for indoor VLC and future smart lighting systems. SINR values were found to be too low. This was due to incorrect grouping of noise and signal ADC readings. Models were not derived for case III due to the high number of errors in the channel.

Chapter 5

Outdoor Modelling

5.1   Introduction

This part of the VLC channel modelling research focuses on outdoor VLC. More specifically, this work models an outdoor channel which could potentially be used for V2V and V2I VLC at night, and for a specific wavelength band. This band includes colours of typical car rear lights which could be used for VLC. The channel models developed are also based on experimental results in different environments or scenarios.

Firstly, the design of the system used for collecting experimental readings is presented. Then, the experimental procedure is outlined and each testing scenario is presented. Results and analysis are then given followed by a conclusion. The techniques used to determine the outdoor channel models are similar to those used to determine the outdoor channel models.

5.2   System Description

The design of the outdoor sensing equipment relies on the IEEE 802.15.7 short-range wireless optical communication using visible light (refer to Chapter 2, Section 2.2). The focus is on the 200 kHz frequency that is used for outdoor VLC. Figure 5.1 shows an overview of the major modules in the outdoor sensing system. Optical signals are sensed, filtered optically, amplified and then filtered again electronically. Sampling takes place on an Arduino microcontroller, following which, the samples
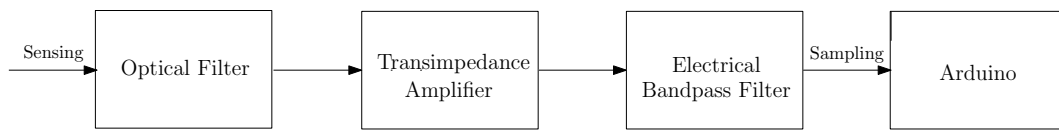
Figure 5.1: Flow diagram of outdoor sensor system.

are uploaded to MATLAB on a PC for further processing. This process is discussed in more detail in the following subsections.
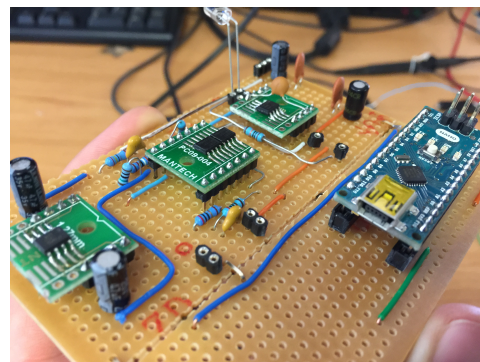
5.2.1   Optical Sensing and Filtering

A lens with 12 cm diameter and focal length of 25 cm is used for the optical sensing. This particular lens was used as it was inexpensive and readily available. The lens and the sensing equipment casing is shown in Figure 5.2(a). The reason for using a large lens is because in an outdoor V2V communication application, the incoming light signals would not be precisely in the LoS. Thus, a larger lens is required in order to capture more light from the environment.

The rear lights of cars include red brake lights and orange indicator lights. These are the LED lights that could potentially be used for V2V VLC. As such, all colours except for red and orange need to be filtered. This was done using a slit of readily available transparent polymethyl methacrylate (commonly known as Perspex) which was placed in front of the photodiode in the sensing equipment. There are several Perspex colours within the red and orange spectrum available for use. Each of these have different absorption characteristics. The names of these filter colours were obtained from the manufacturer. Figure 5.3 gives a comparison of these filters along with the spectral band of a red rear car light. The spectrum for this red light was
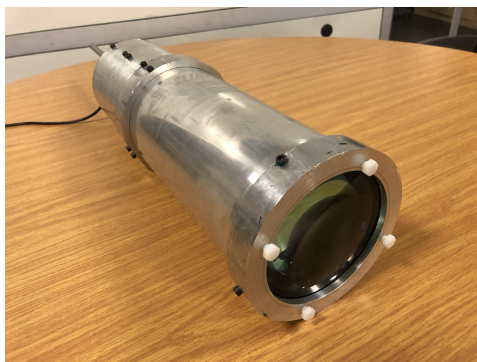
(a) Photo of outdoor optical sensor   (b) Electrical hardware with filter.
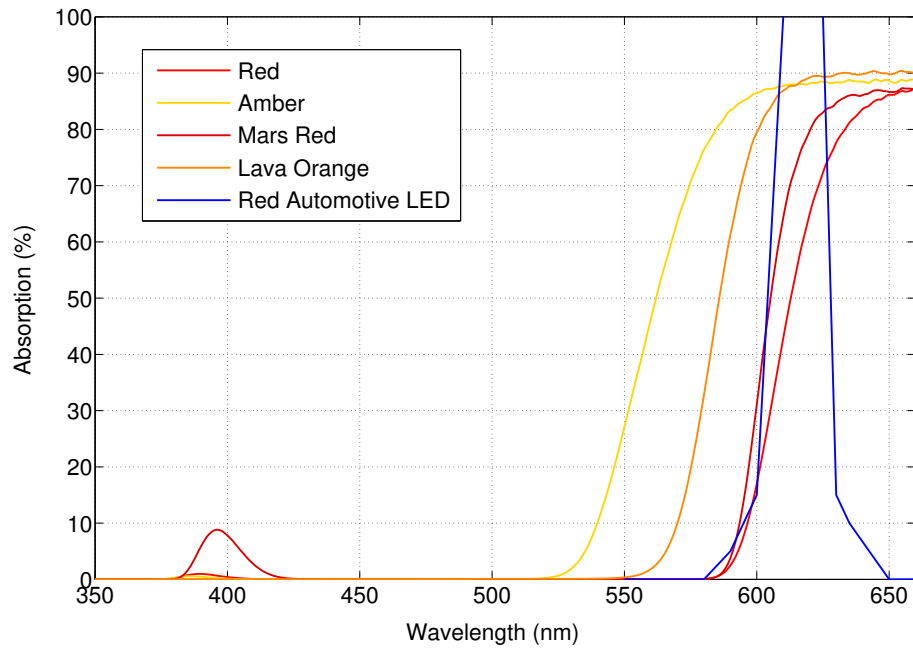
Figure 5.2: Outdoor sensor hardware.

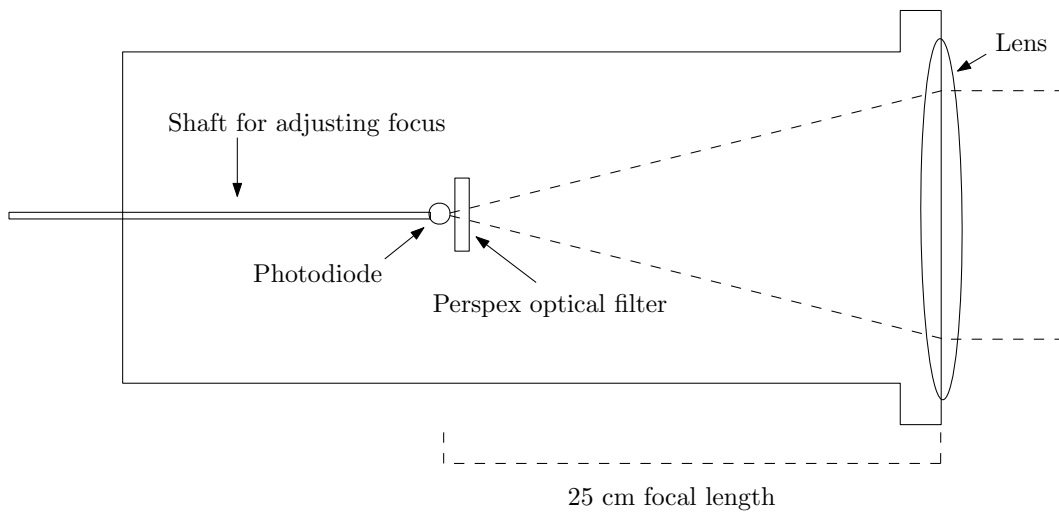**Figure 5.3:** Comparison of optical filters shown with red automotive LED spectrum.

Figure 5.4: Optical sensor diagram

obtained from [77]. The characteristics of each of the filters were measured. Figure 5.3 shows that the Lava Orange colour provides the best amount of absorption for red and orange, as well as for the spectrum of the car LED light. Figure 5.4 shows a cross section of the optical sensor. The photodiode and optical filter are attached to the end of a movable shaft. The shaft can slide to adjust the position of the photodiode along the focal length, if required.

5.2.2 Electrical Amplification and Filtering

Figure 5.5 shows the circuit diagram for the electrical component of the sensing system. Following the optical filter, the optical signals are sensed by an SFH 206 K silicon PIN photodiode. The current signals are then converted to voltage signals using an OPA380 TIA. The gain of this TIA is lower than is required so that the TIA does not reduce the input bandwidth. As such, it is cascaded with a post-amplifier which brings the gain to a desired value. This in turn is followed by an active second order Butterworth bandpass filter with center frequency at approximately 200 kHz, which is the frequency of interest as per the IEEE standard.

5.2.3 Data Processing

Sampling takes place using the Arduino Nano's ADC. The ADC values are uploaded to MATLAB where the threshold values and error sequences are calculated. Each of the samples are used as discrete points for the generation of the models. In order to determine whether a given discrete point is an error or error-free state, a threshold had to be chosen. This was based on the three-sigma rule commonly used for anomaly detection. Any discrete point with an ADC reading above the three-sigma value is considered as an error state. Any reading below the three-sigma value is considered an error-free state. Using this rule and the sampled ADC sequence gives the error sequence needed as one of the inputs to the Baum-Welch algorithm and ultimately the generation of the Fritchman models.
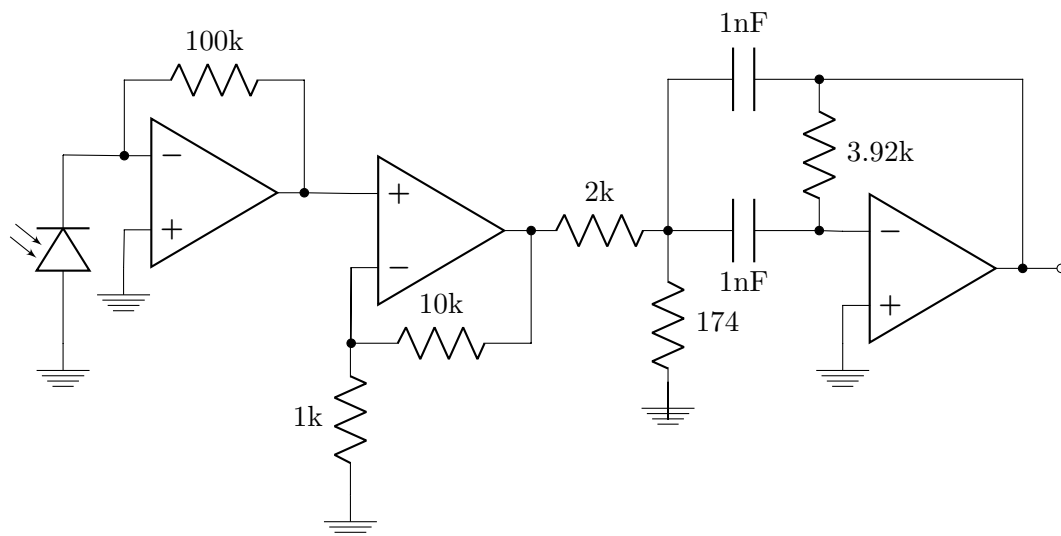

Figure 5.5: Amplifier and filter circuit of the outdoor VLC sensor.

5.3   Experimental Procedure

The sensing equipment was mounted on the dashboard of a car. Sensing was carried out multiple times along four different routes at night-time between 19:30 and 21:30. Each of these routes were on different road environments with varied types of lighting from both infrastructure and vehicles. Each of these environments had a different vehicle speed associated with them. A variation in routes and environments were chosen in an attempt to provide different types of channels that V2V and V2I VLC would be exposed to.

Below are the four routes with descriptions of the types of static and dynamic ambient light. Figures 5.6 - 5.9 include photographs of the routes as well as a GPS mapping of the route that was travelled. GPS routes and speeds were recorded from a smartphone in real-time.
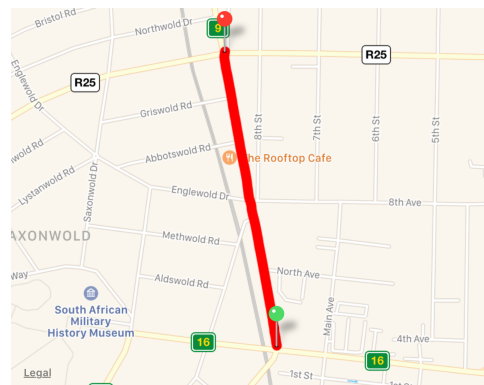

(a) Photo.
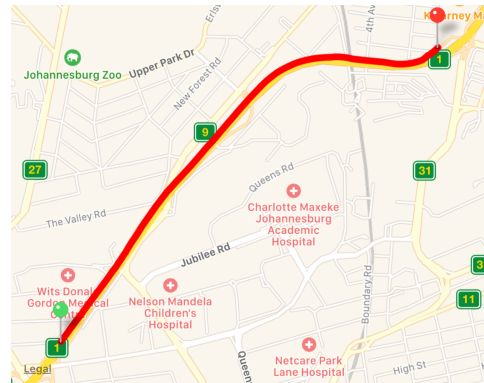
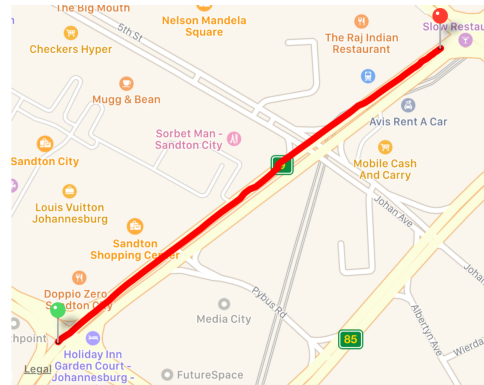**(b)** Route. (©1992-2018 TomTom)

Figure 5.6: Freeway testing route

(a) Photo.

(b) Route. (©1992-2018 TomTom)

Figure 5.7: Commercial testing route
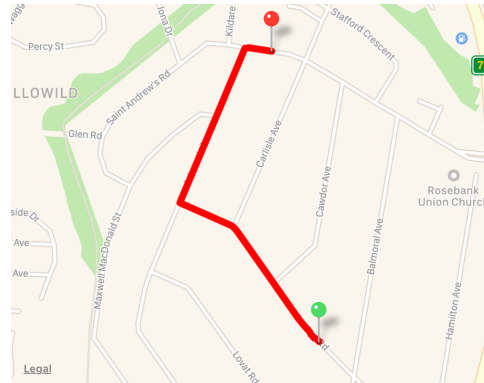
(a) Photo.

(b) Route. (©1992-2018 TomTom)

Figure 5.8: CBD testing route.

(a) Photo.

(b) Route. (©1992-2018 TomTom)

Figure 5.9: Residential testing route

1. **Freeway**: large, bright freeway lights and lit-up billboards with moderate amount of traffic - see Figure 5.6(a).

2. **Commercial**: smaller street lights with some small billboards and low amount of traffic - see Figure 5.7(a).

3. **Central Business District** (CBD) or city: small street lights, many bright billboards and some large LED screens; building lights and moderate traffic - see Figure 5.8(a).

4. **Residential**: small street lights, no traffic, small lights from houses - see Figure 5.9(a).

Experiments were carried out on two evenings, each of which were a weekday. On these evenings, each of the routes were travelled three times while the sensor collected data. The total time for these tests were two minutes which equated to 100,000

discrete samples. The distance and average speed that the vehicle travelled along each route were made to be as close as possible to each other for each individual test. In an attempt to quantify the amount of light the sensor was exposed to, a lux meter was used to record the illuminance within the car where the sensor was placed. As the illuminance would change along the testing route, an illuminance range was recorded.

5.4   Results and Analysis

This section presents and discusses results of the two aspects of channel modelling. Firstly, the EFRD plots are presented with a discussion on some of the differences and correlations between these plots. Secondly, the Fritchman models developed from the EFRD sequences are presented.

5.4.1   Error-free Run Distributions

Figures 5.10, 5.11, 5.12 and 5.13 show the EFRD of the error sequences for the freeway, commercial, CBD and residential routes respectively. The graphs are plotted in such a way to highlight the tests taken on each of the two days. The blue hue EFRD plots are for the first test, and the orange hue EFRD plots are for the second test. The plots show differences between the test sets on each of these days.

The freeway EFRD plots (Figure 5.10) show some grouping in the lower error-free intervals, but deviate as the interval length increases. The test set from each of the days group together at these higher intervals. The commercial EFRD plots (Figure 5.11) similarly group together based on the test day. However, there are some significant deviation in the lower intervals. The first test (blue) showed vastly different distributions, yet the second tests (orange) followed a similar pattern throughout the distribution. The CBD EFRD plots (Figure 5.12) also have grouping in at higher intervals and little correlations between the tests at lower interval lengths, except for Test 1-2 and 2-3 which show some similarity. Finally, the residential EFRD plots (Figure 5.13) show the greatest correlation between the first set of tests (blue). At the lower error-free intervals, all three of the tests that took place showed a similar pattern in error-free runs, even though there is some offset between the patterns. The second group of tests do not show much correlation.

Tests that took place at higher speeds, such as the freeway, had a greater probability
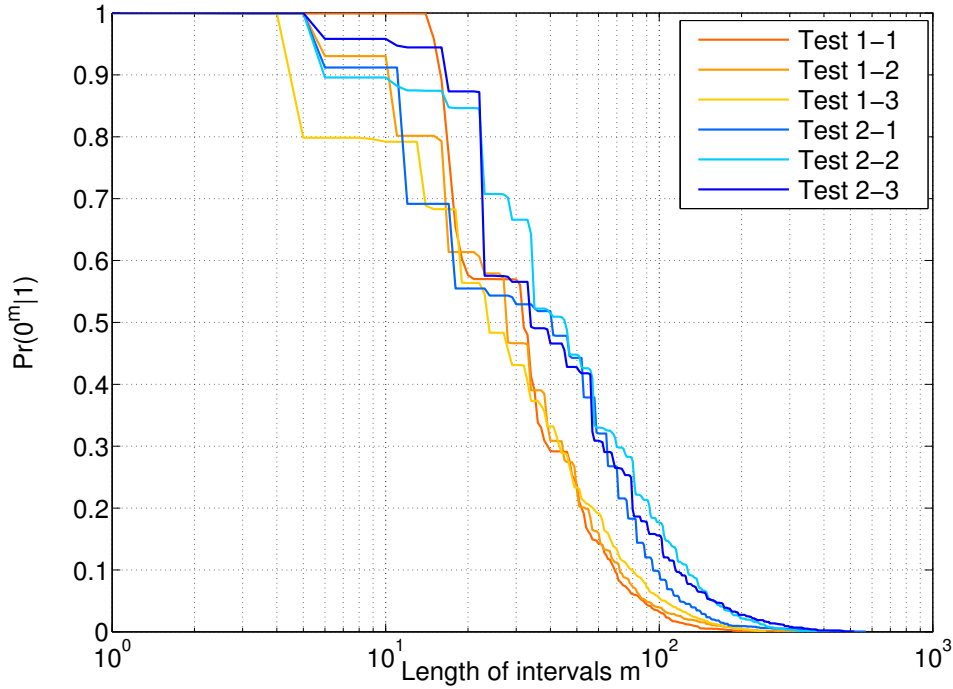
Figure 5.10: Freeway error-free run distributions.

of longer intervals. The slowest travelled route, which was the residential route, has the opposite of this. Probabilities of error-free runs decrease significantly at intervals as low as 2. This can be attributed to the Doppler shift from the ambient light.

5.4.2 Channel Models

Tables 5.1, 5.2, 5.3 and 5.4 show the resultant, three-state Fritchman channel models for the freeway, commercial, CBD and residential environments. The same initial model parameters used in the indoor modelling were also used for this outdoor modelling. These tables also include the MSE and χ^2 value comparisons of the model and IID EFRDs. Almost all of these models (except the first one in Table 5.1 and two in Table 5.3) have the $a_{33} = 0$, similar to some of the results for the indoor channel models for case II. Again, this shows that the error-sequences do not contain any consecutive errors. The tables also show that the models did not perform significantly better than the simple IID model. This is evident by the number of MSE and χ^2 values that are lower for the Fritchman models than for the IID models.

Figure 5.14 show comparisons between the illuminance that the sensor was exposed to in different tests. The figure shows the peak illuminance values (lux) that were
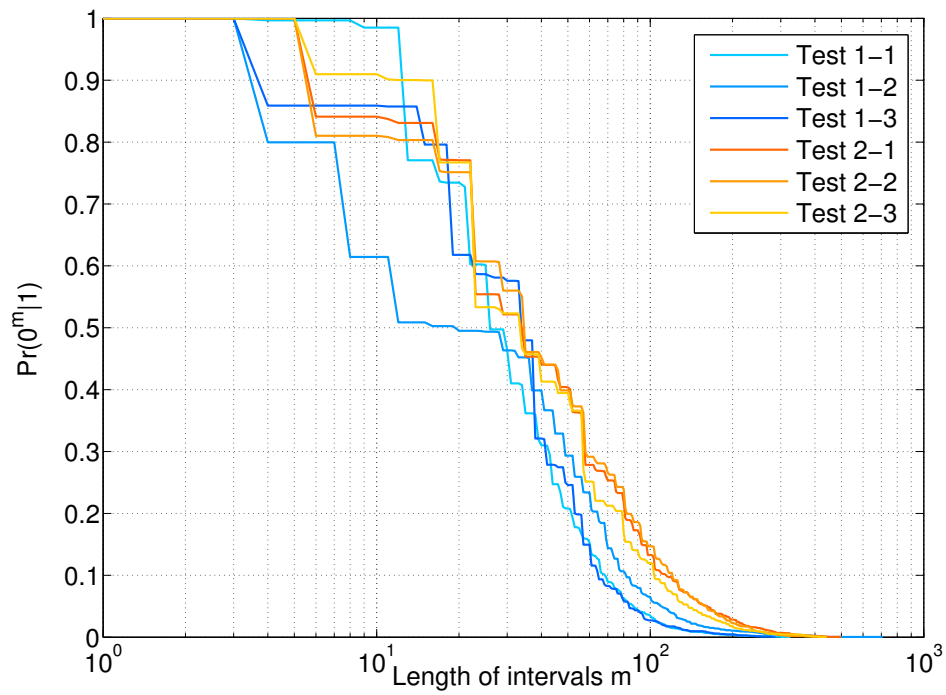
Figure 5.11: Commercial error-free run distributions.
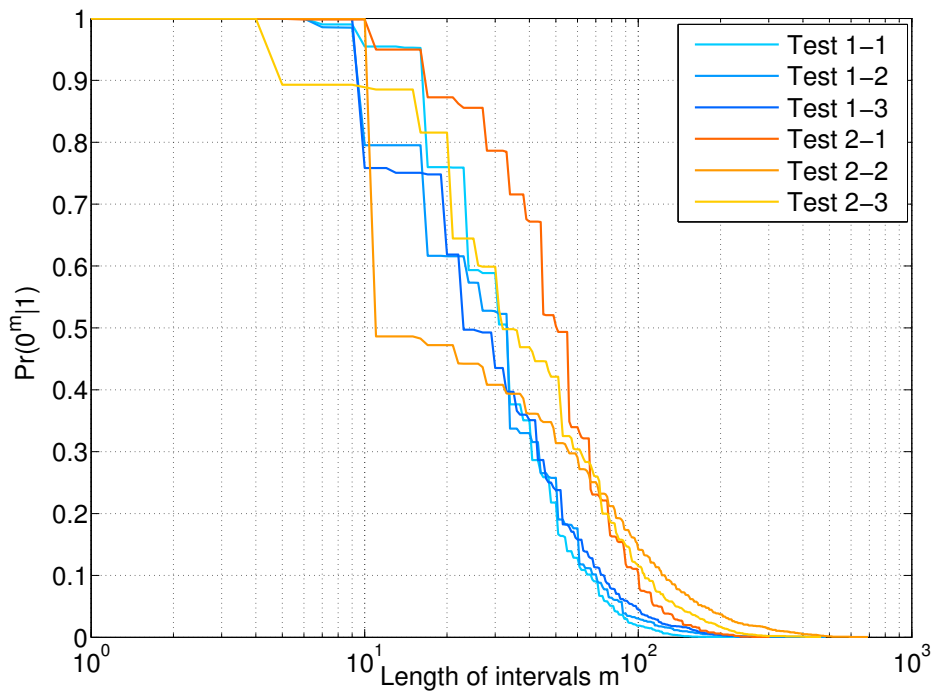

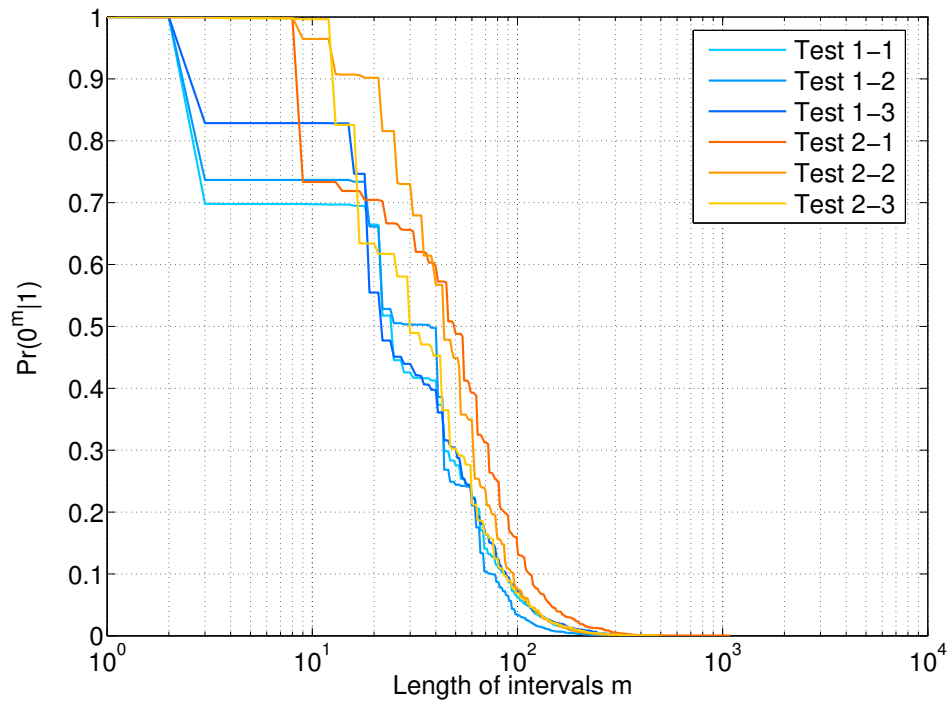**Figure 5.12:** CBD error-free run distributions.

Figure 5.13: Residential error-free run distributions.

measured. Between the groups of three tests, the illuminance values do not vary much. However, it is evident that on the different testing days, the illuminance varied significantly. This is a possible explanation for why there are different results on different days.

Table 5.1: Modelling results for the freeway environment.

Illuminance (lux)	Transition probabilities							MSE		χ^2	
	a_{11}	a_{13}	a_{22}	a_{23}	a_{31}	a_{32}	a_{33}	IID	Model	IID	Model
0.07-unknown [1]	0.9724	0.0276	0.9723	0.0277	0.6493	0.3375	0.0132	3.44E-03	3.54E-03	4.4557	3.8504
0.07-3.78	0.9731	0.0269	0.9709	0.0291	0.6458	0.3542	0.0000	8.08E-04	8.97E-04	1.7338	1.6365
0.07-8.89	0.9753	0.0247	0.9628	0.0372	0.6369	0.3631	0.0000	2.51E-04	2.27E-04	0.1754	0.1761
0.20-2.00	0.9805	0.0195	0.9681	0.0319	0.7891	0.2109	0.0000	9.78E-04	1.05E-03	2.0859	1.5331
0.20-2.96	0.9833	0.0167	0.9807	0.0193	0.8265	0.1735	0.0000	5.31E-04	6.03E-04	1.5384	1.3133
0.90-1.97	0.9832	0.0168	0.9784	0.0216	0.7616	0.2384	0.0000	1.02E-03	1.07E-03	1.2923	1.8955

[1]unintentionally omitted during measurements

Table 5.2: Modelling results for the commercial environment.

Illuminance (lux)	Transition probabilities							MSE		χ^2	
	a_{11}	a_{13}	a_{22}	a_{23}	a_{31}	a_{32}	a_{33}	IID	Model	IID	Model
0.07-9.12	0.9720	0.0280	0.9716	0.0284	0.6420	0.3580	0.0000	1.73E-03	1.60E-03	3.7054	2.3640
0.04-9.67	0.9801	0.0199	0.8345	0.1655	0.6930	0.3070	0.0000	1.46E-03	8.94E-04	1.6358	1.7907
0.06-8.35	0.9723	0.0277	0.9716	0.0284	0.6876	0.3124	0.0000	1.84E-03	2.04E-03	3.7555	3.1797
0.21-2.97	0.9832	0.0168	0.9695	0.0305	0.7308	0.2692	0.0000	3.78E-04	3.11E-04	0.8575	0.4361
0.22-3.50	0.9830	0.0170	0.9683	0.0317	0.7707	0.2293	0.0000	2.34E-04	3.26E-04	0.1851	0.3126
0.30-3.45	0.9809	0.0191	0.9748	0.0252	0.7201	0.2799	0.0000	7.20E-04	8.09E-04	0.9423	1.0793

Table 5.3: Modelling results for the CBD environment.

Illuminance (lux)	Transition probabilities							MSE		χ^2	
	a_{11}	a_{13}	a_{22}	a_{23}	a_{31}	a_{32}	a_{33}	IID	Model	IID	Model
0.04-0.12	0.9721	0.0279	0.9721	0.0279	0.6823	0.3177	0.0000	4.61E-03	5.20E-03	15.4169	14.5457
0.06-0.13	0.9722	0.0278	0.9709	0.0291	0.6447	0.3550	0.0004	1.17E-03	1.25E-03	2.8312	2.4393
0.06-0.13	0.9730	0.0270	0.9708	0.0292	0.6349	0.3647	0.0004	1.23E-03	1.06E-03	1.2789	0.8057
0.27-2.38	0.9820	0.0180	0.9819	0.0181	0.8726	0.1274	0.0000	5.72E-03	5.97E-03	21.5855	19.1822
0.31-2.67	0.9874	0.0126	0.9326	0.0674	0.5332	0.4668	0.0000	2.32E-03	1.00E-03	5.2550	1.6962
0.33-2.04	0.9810	0.0190	0.9766	0.0234	0.7617	0.2383	0.0000	4.08E-04	3.62E-04	0.9460	0.5047

Table 5.4: Modelling results for the residential environment.

| Illuminance (lux)	Transition probabilities							MSE		χ^2	
	a_{11}	a_{13}	a_{22}	a_{23}	a_{31}	a_{32}	a_{33}	IID	Model	IID	Model
0.03-0.06	0.9790	0.0210	0.5005	0.4995	0.7635	0.2365	0.0000	8.83E-04	1.04E-03	0.6488	2.6986
0.06-0.27	0.9757	0.0243	0.8932	0.1068	0.8340	0.1660	0.0000	1.37E-03	1.96E-03	2.1383	4.5131
0.06-0.09	0.9787	0.0213	0.9602	0.0398	0.6591	0.3409	0.0000	4.74E-04	4.59E-04	0.6458	0.9382
0.04-1.16	0.9832	0.0168	0.9705	0.0295	0.8816	0.1184	0.0000	9.31E-04	1.05E-03	1.9354	2.4720
0.02-1.09	0.9807	0.0193	0.9806	0.0194	0.8291	0.1709	0.0000	2.60E-03	2.80E-03	11.0231	10.4231
0.04-2.27	0.9775	0.0225	0.9754	0.0246	0.7035	0.2965	0.0000	7.63E-04	8.34E-04	1.3953	2.3335
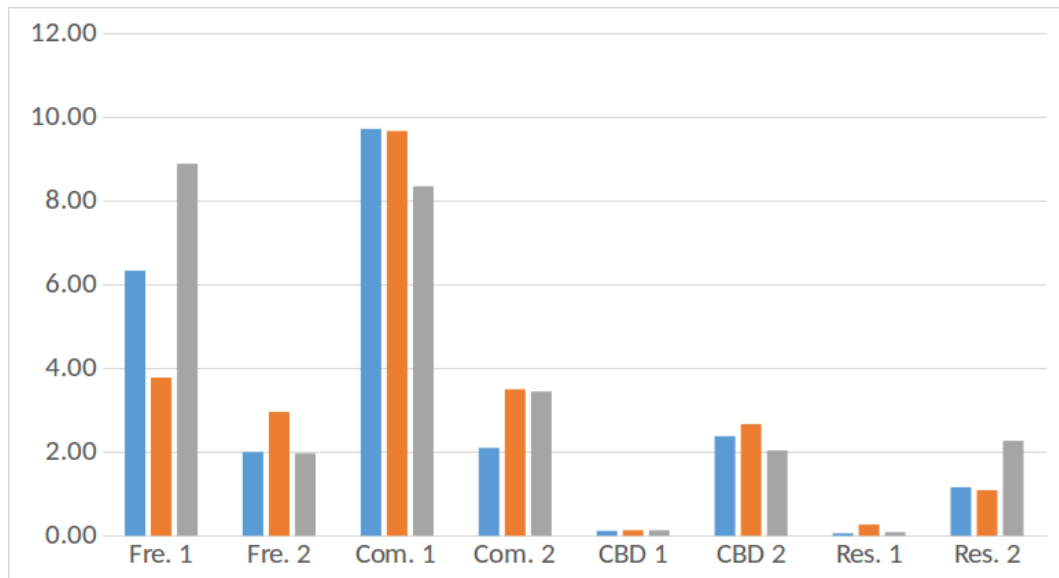
Figure 5.14: Comparison of maximum lux for each test.

5.4.3   Discussion

The results showed that there is little correlation in error-state distributions for each
environment. The exception to this were the first residential route tests and the
second commercial route tests, which did show similar patterns. These variations
can be attributed to the differences in environmental conditions and testing routes,
despite the same route with the same average speeds being travelled. In general,
the artificial light along these routes are inconsistent. A great contributor to these
inconsistencies were the lights from other vehicles, which changed based on traffic
flows. This leads to inconsistencies in error state distributions and models. This is
further reinforced by the variations in the illumination values. However, illumination
does not take into account the 200 kHz frequency that the sensor was designed to
sense. For example, the CBD route may have had a lower illuminance, but the route
was the most diverse in terms of artificial light sources, such as large advertising
screens and building lights; which could possibly include more in-band interference.

5.4.4   Conclusion

Models for the outdoor environment similarly did not provide good approximations
of the channel. This was also due to a lack of error clusters. This is mainly due
to the vast inconsistencies in each environment, even along the same testing route.
These are most likely a result of the differences in traffic flow between each test.
Illuminance readings highlighted some of these differences in what the sensor was

exposed to. The EFRD did show some insight into how the speed of the car during tests can be attributed to the Doppler shift.

Chapter 6

Conclusion

6.1 Research Summary

The research presented herein aims to answer the following research question:

What is the statistical distribution of error states for smart lighting indoor VLC and outdoor V2V VLC channels, from differing scenarios of noise and interference, based on semi-hidden Markov models?

To begin addressing this question, in Chapter 2 the literature review firstly gave an overview of the field of VLC and a high level view of the state of the art. Aspects of the IEEE VLC standard that related to some of the hardware used in the research were given. General channel models currently employed in the field of VLC were presented. The literature review then presented research that has been done on indoor and outdoor VLC channels, as well as an in depth treatment of research done using the Baum-Welch algorithm, HMMs and the Fritchman model. Chapter 3 presented details on the techniques employed in determining the statistical distribution of VLC channel error states. This includes an in-depth treatment of the Baum-Welch algorithm and the Fritchman model.

Chapters 4 and 5 present the indoor and outdoor components of the VLC channel modelling respectively. Each of these sections included descriptions of the hardware that was designed for collection of experimental results, as well as the experimental methodologies, modelling results and analysis. Three-state SHMM models (also known as Fritchman models) were derived from experimental measurements by using the Baum-Welch algorithm. Analysis of the models was done using EFRD and log-likelihood plots. Comparisons of the models to IID sequences were made using

χ^2 tests and MSE.

The outputs of the research include a journal paper based on the indoor channel modelling that is currently under review; and a paper based on the outdoor channel modelling that is currently still under development.

6.2   Recommendations for Possible Future Work

Below are recommendations for possible future work and research, building upon the research and conclusions presented herein:

- Optimal OOK threshold detection in the presence of pseudo-random interfering signal with the same modulation scheme.

- Interference mitigation techniques for co-existing VLC and smart lighting systems.

- SINR measurement in the presence of interfering PWM signals.

- Outdoor channel modelling in a more deterministic environment.

- Impact of vehicle speed in V2V VLC.

- Alternative discrete channel modelling techniques for channels without error-clusters.

- Comparison of other models for VLC channels, particularly GE and Fritchman models.

- Investigation into considering the maximum transmit power allowed between neighbouring transmitting LEDs.

6.3   Conclusion

The research presented herein showed that the Fritchman model is able to model VLC channels in both indoor and outdoor environments. However, the models do not provide a significantly better fit compared to simpler IID models. An exception to this is the indoor VLC environment that only had background noise and interference, where the models performed better. These particular models could be used for

software simulations of VLC channels. The outdoor environments proved difficult to model due to variations in outdoor lighting conditions, specifically due to other car lights. It is recommend that more stable outdoor channels are investigated as a starting point. The research highlighted the impact that interfering PWM signals have in a smart lighting system use case. The error patterns observed showed correlations between the PWM duty cycles and error-free runs. These can potentially be used for designing error control codes and interference avoidance and mitigation techniques.

Bibliography

[1] P. Pathak, X. Feng, P. Hu, and P. Mohapatra. "Visible Light Communication, Networking and Sensing: A Survey, Potential and Challenges." *IEEE Communications Surveys & Tutorials*, vol. 17, no. 4, pp. 2047–2077, 2015.

[2] A. Sevincer, A. Bhattarai, M. Bilgi, M. Yuksel, and N. Pala. "LIGHTNETs: Smart Lighting and Mobile Optical Wireless Networks - A Survey." *IEEE Communications Surveys & Tutorials*, vol. 15, no. 4, pp. 1620–1641, 2013.

[3] M. Ayyash, H. Elgala, A. Khreishah, V. Jungnickel, T. Little, S. Shao, M. Rahaim, D. Schulz, J. Hilt, and R. Freund. "Coexistence of WiFi and LiFi towards 5G: Concepts, Opportunities, and Challenges." *IEEE Communications Magazine*, , no. 2, pp. 64–71, 2016.

[4] W. Tranter. *Principles of Communication Systems Simulation with Wireless Applications*. Prentice Hall communications engineering and emerging technologies series. Prentice Hall Professional Technical Reference, first ed., 2004.

[5] B. D. Fritchman. "A Binary Channel Characterization Using Partitioned Markov Chains." *IEEE Transactions on Information Theory*, vol. 13, no. 2, pp. 221–227, 1967.

[6] L. E. Baum, T. Petrie, G. Soules, and N. Weiss. "A Maximization Technique Occurring in the Statistical Analysis of Probabilistic Functions of Markov Chains." *The Annals of Mathematical Statistics*, vol. 4, no. 1, pp. 164–171, 1970.

[7] A. Cailean and M. Dimian. "Current Challenges for Visible Light Communications Usage in Vehicle Applications: A Survey." *IEEE Communications Surveys & Tutorials*, vol. 19, no. 4, pp. 2681 – 2703, 2017.

[8] D. Karunatilaka, F. Zafar, V. Kalavally, and R. Parthiban. "LED Based Indoor Visible Light Communications: State of the Art." *IEEE Communications Surveys & Tutorials*, vol. 17, no. 3, pp. 1649–1678, 2015.

[9] IEEE. "IEEE Standard for Local and metropolitan area networks Part 15.7: Short-Range Wireless Optical Communication Using Visible Light.", 2011.

[10] H. Li, X. Chen, B. Huang, D. Tang, and H. Chen. "High Bandwidth Visible Light Communications Based on a Post-Equalization Circuit." *IEEE Photonics Technology Letters*, vol. 26, no. 2, pp. 119–122, 2014.

[11] N. Shrestha, M. Sohail, C. Viphavakit, P. Saengudomlert, and W. S. Mohammed. "Demonstration of Visible Light Communications Using RGB LEDs in an Indoor Environment." In *2010 International Conference on Electrical Engineering/Electronics Computer Telecommunications and Information Technology (ECTI-CON)*, pp. 1159–1163. 2010.

[12] A. Sewaiwar, P. P. Han, and Y. H. Chung. "3 Gbit/s Indoor Visible Light Communications using Optical Diversity Schemes." *IEEE Photonics Journal*, vol. 7, no. 6, 2015.

[13] C. Kamwangala, M. A. Cox, and L. Cheng. "Transmitter power control for a multicarrier visible light communication system." *Transactions on Emerging Telecommunications Technologies*. June 2018, e3453 ett.3453.

[14] F. Wu, C. Lin, C. Wei, C. Chen, Z. Chen, and H. Huang. "3 .22-Gb/s WDM Visible Light Communication of a Single RGB LED Employing Carrier-Less Amplitude and Phase Modulation." In *Optical Fiber Communication Conference and Exposition and the National Fiber Optic Engineers Conference*, pp. 1–3. 2013.

[15] T. Komine and M. Nakagawa. "Fundamental Analysis for Visible-Light Communication System Using LED Lights." *IEEE Transactions on Consumer Electronics*, vol. 50, no. 1, pp. 100–107, 2004.

[16] C. W. Chow, C. Y. Chen, and S. H. Chen. "Enhancement of Signal Performance in LED Visible Light Communications Using Mobile Phone Camera." *IEEE Photonics Journal*, vol. 7, no. 5, 2015.

[17] M. Singleton. "Sony's latest smartphone camera sensor can shoot at 1,000fps.", 2017. URL https://www.theverge.com/circuitbreaker/2017/2/7/14532610/sony-smartphone-camera-sensor-1000-fps. Last accessed: March 2017.

[18] C. Danakis, M. Afgani, G. Povey, I. Underwood, and H. Haas. "Using a CMOS Camera Sensor for Visible Light Communication." In *2012 IEEE Globecom Workshops*, pp. 1244–1248. 2012.

[19] T. Do and M. Too. "Analysis on Visible Light Communication using Rolling Shutter CMOS Sensor." In *International Conference on Information and Communication Technology Convergence (ICTC)*, pp. 755–757. 2015.

[20] H. Lu and Z. Su. "An Indoor Visible Light Communication Model Under the Condition of Multipath Transmission." In *8th International Congress on Image and Signal Processing*, 8, pp. 1137–1141. 2015.

[21] Q. Wang, D. D. Donno, and D. Giustiniano. "Demonstration Abstract: Research Platform for Visible Light Communication and Sensing Systems." In *15th ACM/IEEE International Conference on Information Processing in Sensor Networks (IPSN)*. 2016.

[22] W. Hussain, H. F. Ugurdag, and M. Uysal. "Software Defined VLC System: Implementation and Performance Evaluation." In *4th International Workshop on Optical Wireless Communications*, pp. 117–121. 2015.

[23] L. P. Klaver. *Design of a network stack for directional visible light communication*. Master's thesis, Delft University of Technology, Faculty of Electrical Engineering, Mathematics and Computer Science, 2014.

[24] L. C. Png, L. Chen, S. Liu, and W. K. Peh. "An Arduino-based indoor positioning system (IPS) using visible light communication and ultrasound." *Digest of Technical Papers - IEEE International Conference on Consumer Electronics*, pp. 217–218, 2014.

[25] H. Haas, L. Yin, Y. Wang, and C. Chen. "What is LiFi ?" *Journal of Lightware Technology*, vol. 34, no. 6, pp. 1533–1544, 2015.

[26] P. Chernatanomwong and W. Chantharasena. "Indoor Localisation System Using Visible Light Communication." In *7th International Conference on Information Technology and Electrical Engineering*, pp. 480–483. 2015.

[27] C. Wang, L. Wang, X. Chi, S. Liu, W. Shi, and J. Deng. "The Research of Indoor Positioning Based on Visible Light Communication." *China Communications*, vol. 12, no. 8, pp. 85–92, 2015.

[28] H. Ma, L. Lampe, and S. Hranilovic. "Integration of Indoor Visible Light and Power Line Communication Systems." In *IEEE 17th International Symposium on Power Line Communications and Its Applications*, pp. 291–296. 2013.

[29] J. Song, W. Ding, F. Yang, H. Yang, J. Wang, X. Wang, and X. Zhang. "Indoor Hospital Communication Systems: An Integrated Solution Based Power Line and Visible Light Communication." In *2014 IEEE Faible Tension Faible Consommation*, pp. 1–6. 2014.

[30] T. Yamazato, I. Takai, and H. Okada. "Image-Sensor-Based Visible Light Communication for Automotive Applications." *IEEE Communications Magazine*, , no. 7, pp. 88–97, 2014.

[31] G. Cossu, R. Corsini, A. M. Khalid, S. Balestrino, A. Coppelli, A. Caiti, and E. Ciaramella. "Experimental Demonstration of High Speed Underwater Visible Light Communications." In *2nd International Workshop on Optical Wireless Communications (IWOW)*, pp. 11–15. 2013.

[32] N. Xavier, A. Kumar, and S. K. Panda. "Design, Fabrication and Testing of Smart Lighting System." In *Future Technologies Conference*, pp. 763–768. 2016.

[33] Z. Gassemlooy, L. N. Alves, S. Zvanovec, and M.-A. Khalighi, editors. *Visible Light Communicaions Theory and Applications*. CRC Press, 2017.

[34] K. Lee, H. Park, and J. R. Barry. "Indoor Channel Characteristics for Visible Light Communications." *IEEE Communications Letters*, vol. 15, no. 2, pp. 217–219, 2011.

[35] H. Chun, C.-J. Chiang, and D. C. O'Brien. "Visible light communication using OLEDs: Illumination and channel modeling." *International Workshop on Optical Wireless Communications (IWOW)*, pp. 1–3, 2012.

[36] F. Miramirkhani and M. Uysal. "Indoor Channel Modelling and Characterization for Visible Light Communications." *IEEE Photonics Journal*, vol. 7, no. 6, pp. 1–4, 2015.

[37] F. Miramirkhani, O. Narmanlioglu, M. Uysal, and E. Panayirci. "A Mobile Channel Model for VLC and Application to Adaptive System Design." *IEEE Communications Letters*, vol. 21, no. 5, pp. 1035–1038, 2017.

[38] M. Uysal, F. Miramirkhani, O. Narmanlioglu, T. Baykas, and E. Panayirci. "IEEE 802.15.7r1 Reference Channel Models for Visible Light Communications." *IEEE Communications Magazine*, vol. 55, no. 1, pp. 212–217, 2017.

[39] E. Sarbazi and M. Uysal. "Ray Tracing Based Channel Modeling for Visible Light Communications." In *IEEE 22nd Signal Processing and Communications Applications Conference*, 22, pp. 702–705. 2014.

[40] P. Chvojka, S. Zvanovec, P. A. Haigh, and Z. Ghassemlooy. "Channel Characteristics of Visible Light Indoor Environment." *Journal of Lightwave Technology*, vol. 33, no. 9, pp. 1719–1725, 2015.

[41] P. Luo, Z. Ghassemlooy, H. Le Minh, E. Bentley, A. Burton, and X. Tang. "Fundamental Analysis of a Car to Car Visible Light Communication System." In *2014 9th International Symposium on Communication Systems, Networks and Digital Signal Processing, CSNDSP 2014*, pp. 1011–1016. 2014.

[42] Z. Cui, P. Yue, and Y. Ji. "Study of Cooperative Diversity Scheme Based on Visible Light Communication in VANETs." In *2016 International Conference on Computer, Information and Telecommunication Systems (CITS)*, pp. 1–5. 2016.

[43] W. Viriyasitavat, S. H. Yu, and H. M. Tsai. "Short paper: Channel Model for Visible Light Communications Using Off-the-shelf Scooter Taillight." *IEEE Vehicular Networking Conference, VNC*, pp. 170–173, 2013.

[44] K. Cui, G. Chen, Z. Xu, and R. D. Roberts. "Traffic light to vehicle visible light communication channel characterization." *Applied Optics*, vol. 51, no. 27, pp. 6594–6605, 2012.

[45] L. C. Wu and H. M. Tsai. "Modeling Vehicle-to-Vehicle Visible Light Communication Link Duration with Empirical Data." In *2013 IEEE Globecom Workshops, GC Wkshps 2013*, pp. 1103–1109. 2013.

[46] L. Rabiner. "A tutorial on hidden Markov models and selected applications in speech recognition." *Proceedings of the IEEE*, vol. 77, no. 2, pp. 257–286, 1989.

[47] S. E. Levinson, L. R. Rabiner, and M. M. Sondhi. "An Introduction to the Application of the Theory of Probabilistic Functions of a Markov Process to Automatic Speech Recognition." *The Bell System Technical Journal*, vol. 62, no. 4, pp. 1035–1074, 1983.

[48] X. Zhang and J. S. Mason. "Improved Training using Semi-hidden Markov Models in Speech Recognition." In *International Conference on Acoustics, Speech, and Signal Processing*, pp. 306–309. 1989.

[49] C. V. Wright, L. Ballard, S. E. Coull, F. Monrose, and G. M. Masson. "Spot me if you can: Uncovering spoken phrases in encrypted VoIP conversations." *Proceedings - IEEE Symposium on Security and Privacy*, pp. 35–49, 2008.

[50] M. Erkurt and J. G. Proakis. "Joint Data Detection and Channel Estimation for Rapidly Fading Channels." In *IEEE Global Telecommunications Conference, GLOBECOM*, pp. 910–914. 1992.

[51] S. Sivaprakasam and K. S. Shanmugan. "An Equivalent Markov Model for Burst Errors in Digital Channels." *IEEE Transactions on Communications*, vol. 43, no. 2, pp. 1347–1355, 1995.

[52] K. Choi and J.-N. Hwang. "Baum-Welch Hidden Markov Model Inversion For Reliable Audio-To-Visual Conversion." In *IEEE Third Workshop on Multimedia Signal Processing*, pp. 175–180. 1999.

[53] P. M. Baggenstoss. "A Modified Baum Welch Algorithm for Hidden Markov Models with Multiple Observation Spaces." *IEEE Transactions of Speech and Audio Processing*, vol. 9, no. 4, pp. 411–416, 2001.

[54] W. Turin and M. M. Sondhi. "Modeling Error Sources in Digital Channels." *IEEE Journal on Selected Areas in Communications*, vol. 11, no. 3, pp. 340–347, 1993.

[55] X. Liu, C. Gong, S. Li, and Z. Xu. "Signal Characterization and Receiver Design for Visible Light Communication under Weak Illuminance." *IEEE Communications Letters*, vol. 20, no. 7, pp. 1349 – 1352, 2016.

[56] A. D. Familua and L. Cheng. "Modeling of In-House CENELEC A-Band PLC Channel using Fritchman Model and Baum-Welch algorithm." In *ISPLC 2013 - 2013 IEEE 17th International Symposium on Power Line Communications and Its Applications, Proceedings*, pp. 173–178. 2013.

[57] A. D. Familua, A. R. Ndjiongue, K. Ogunyanda, L. Cheng, H. C. Ferreira, and T. G. Swart. "A Semi-Hidden Markov Modeling of a Low Complexity FSK-OOK In-House PLC and VLC Integration." In *2015 IEEE International Symposium on Power Line Communications and Its Applications, ISPLC 2015*, pp. 199–204. 2015.

[58] A. R. Ndjiongue, H. C. Ferreira, J. Song, F. Yang, and L. Cheng. "Hybrid PLC-VLC channel model and spectral estimation using a nonparametric approach." *Transactions on Emerging Telecommunications Technologies*, vol. 28, no. 12, p. e3224.

[59] J. A. W. Tina, A. J. Snyders, and H. C. Ferreira. "Implementation of a Gap Recorder for Measuring Impulsive Noise Error Distributions in Power Line Communications Using the Fritchman Model." In *2012 IEEE International Symposium on Power Line Communications and Its Applications, ISPLC 2012*, pp. 374–379. 2012.

[60] A. D. Familua, K. Ogunyanda, T. G. Swart, H. C. Ferreira, R. Van Olst, and L. Cheng. "Narrowband PLC channel modeling using USRP and PSK

modulations." *IEEE ISPLC 2014 - 18th IEEE International Symposium on Power Line Communications and Its Applications*, pp. 156–161, 2014.

[61] E. Costamagna, L. Favalli, P. Gamba, E. Passi, F. Babich, D. Elettronica, and U. Pavia. "An Hidden Markov Model for Indoor Channel Based on Experimental Data." In *Conference on Antennas and Propagation for Wireless Communications, 2000 IEEE-APS*, pp. 69–72. 2000.

[62] A. Van Heerden and H. C. Ferreira. "Modelling of Frequency Hopped VHF Channels in an Urban Environment and Error Correction on the Channel." In *South African Symposium on Communications and Signal Processing*, pp. 189–194. 1992.

[63] F. Swarts and H. C. Ferreira. "Modeling and Performance Evaluation of Mobile VHF Radio Channels Employing FSK, DPSK, QPSK and 8-ary PSK as Modulation Scheme." In *IEEE Global Telecommunications Conference*, 1, pp. 1935–1939. 2000.

[64] O. A. Dobre, I. Bdescu, and M. Minea. "Markov Characterization of a Digital Channel." In *5th International Conference on Telecommunications in Modern Satellite, Cable and Broadcasting Service, TELSIKS 2001*, vol. 2, pp. 579–580. 2001.

[65] J. Garcia-Frias and P. M. Crespo. "Hidden Markov Models for Burst Error Characterization in Indoor Radio Channels." *IEEE Transactions on Vehicular Technology*, vol. 46, no. 4, pp. 1006–1020, 1997.

[66] J.-Y. Chouinard, M. Lecours, and G. Y. Delisle. "Estimation of Gilbert's and Fritchman Models Parameters Using the Gradient Method for Digital Mobile Radio Channels." *IEEE Transactions on Vehicular Technology*, vol. 37, no. 3, pp. 158–166, 1988.

[67] P. van Rooyen, M. Lotter, F. Swartz, and R. Kohno. "Partitioned Markov Models for DS/SSMA." In *Fourth IEEE Conference on Universal Personal Communications*, pp. 635–639. 1994.

[68] P. G. W. van Rooyen and H. C. Ferreira. "Mathematical Channel Models for Spread Spectrum Data Communications." In *Proceedings of IEEE Pacific Rim Conference on Communications, Computers and Signal Processing*, pp. 782–785. 1993.

[69] C. Pimentel. "Modeling Burst Channels Using Partitioned Fritchman's Markov Models." *IEEE Transactions on Vehicular Technology*, vol. 47, no. 3, pp. 885–899, 1998.

[70] J. S. Swarts and H. C. Ferreira. "On the Evaluation and Application of Markov Channel Models in Wireless Communications." *IEEE Vehicular Technology Conference*, vol. 50, no. 1, pp. 117–121, 1999.

[71] O. S. Salih, C.-X. Wang, B. Ai, and R. Mesleh. "Adaptive Generative Models for Digital Wireless Channels." *IEEE Transactions on Wireless Communications*, vol. 13, no. 9, pp. 5173–5182, 2014.

[72] A. I. Drukarev and K. P. Yiu. "Performance of Error-Correcting Codes on Channels with Memory." *IEEE Transactions on Communications*, vol. COM-34, no. 6, pp. 513–521, 1986.

[73] A. J. C. Moreira, R. T. Valadas, and A. M. de Oliveira Duarte. "Characterisation and Modelling of Artificial Light Interference in Optical Wireless Communication Systems." In *International Symposium on Personal, Indoor and Mobile Radio Communications*, vol. 1, pp. 326–331. 1995.

[74] M. Rahaim and T. D. C. Little. "Optical Interference Analysis in Visible Light Communication Networks." In *2015 IEEE International Conference on Communication Workshop (ICCW)*, pp. 1410–1415. 2015.

[75] R. C. Kizilirmak and Y. H. Kho. "Mitigation of Illumination Interference Caused by PWM Dimming in OFDM Based Visible Light Communication Systems." In *2015 2nd International Conference on Computer, Communications, and Control Technology*, pp. 489–492. 2015.

[76] E. N. Gilbert. "Capacity of a Burst-Noise Channel." *The Bell System Technical Journal*, vol. 39, no. 5, pp. 1253–1265, 1960.

[77] B. Turan and S. Ucar. *Visible Light Communications*. Rijeka, Croatia: IntechOpen Publishing, first ed., July 2017.

Appendix A

SNR and SINR Calculations

For the indoor channel modelling, the calculation of the Signal-to-Noise Ratio (SNR) and Signal-to-Interference-Plus-Noise Ratio (SINR) formed a significant part of the experimental procedure and modelling. This was for two reasons. Firstly, the SNR readings gave a metric for measuring the change in transmit power. Reading the actual power of the LED was not practical. Secondly, the SNR values are used as a point of reference for each model, with each model having a corresponding SNR.

With these factors in mind, it was essential to have reasonable SNR readings. As such, the SNR values from the error sequences of indoor experiments were used to plot a BER curve. Figure A.1 shows a comparison of the actual BER with the theoretical BER for OOK VLC. The experimental BER varies from the actual BER by up to 2 dB and shows a worse performance which is expected.

The theoretical BER for an OOK VLC [15] was calculated using:

$$\text{BER} = Q(\sqrt{\text{SNR}}) \tag{A.1}$$

For case I, SNR was calculated using:

$$\text{SNR} = \frac{\sigma_S^2}{\sigma_B^2} \tag{A.2}$$

The σ_B^2 term includes the background, thermal and shot noises as well ($\sigma_{shot}^2 + \sigma_{thermal}^2$). This measurement was taken in single readings for each test. For case II, the SINR was calculated using three measurements. A description of each is followed by the relevant equation below. The first and second measurements are used to
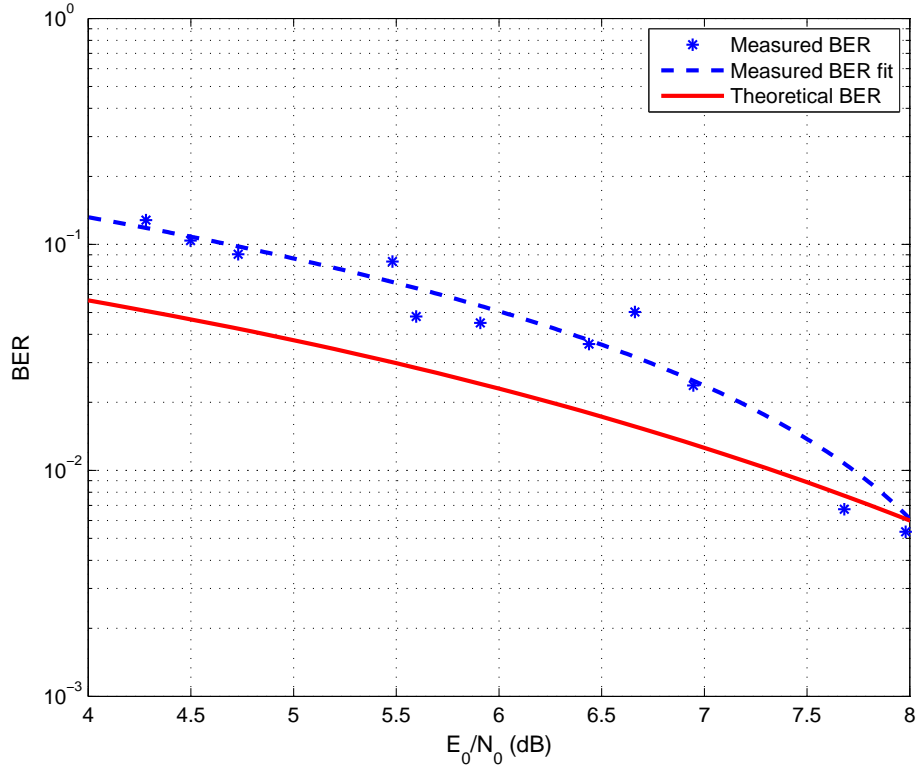
Figure A.1: Bit-error rate comparison

get the signal component while the third measurement is used to get the noise and interference components.

1. PWM signal is active:

$$\sigma_1^2 = \sigma_B^2 + \sigma_{PWM}^2 \tag{A.3}$$

2. PWM signal is active and the source is transmitting a random signal:

$$\sigma_2^2 = \sigma_B^2 + \sigma_{PWM}^2 + \sigma_S^2 \tag{A.4}$$

3. PWM signal is active with measurements X_i grouped based on whether the PWM signal is high or low.

$$\sigma_3^2 \Rightarrow \{X_i\} : T_{low} \tag{A.5}$$

$$\sigma_4^2 \Rightarrow \{X_i\} : T_{high} \tag{A.6}$$

$$\frac{\sigma_3^2 + \sigma_4^2}{2} = \overline{\sigma}_{PWM}^2 + \sigma_B^2 \tag{A.7}$$

Using the above measurements, the final SINR is then calculated by:

$$\text{SINR} = \frac{2(\sigma_2^2 - \sigma_1^2)}{\sigma_3^2 + \sigma_4^2} \tag{A.8}$$

Appendix B

Comparison of Statistical Results

As part of the evaluation of the goodness-of-fit of the channel models, the MSE and chi-squared test were used. Below are plots of comparisons of these values for each of the models at different SNR/SINR values. This gives an indication of the accuracy of the models as a function of SNR/SINR.

The figures include plots of P_e vs χ^2 (Figures B.1, B.5, B.9), P_e vs MSE (Figures B.2, B.6, B.10), SINR vs χ^2 (Figures B.3, B.7, B.11), and SINR vs MSE (Figures B.4, B.8, B.12) for the 25 %, 50 % and 75 % duty cycles interference. The two sets of data for these plots are the IID and model χ^2 and MSE values. Variations between these two values were larger for lower error probabilities and higher SINR values, where (in most cases) the models provided a better goodness-of-fit compared to the IID sequence.
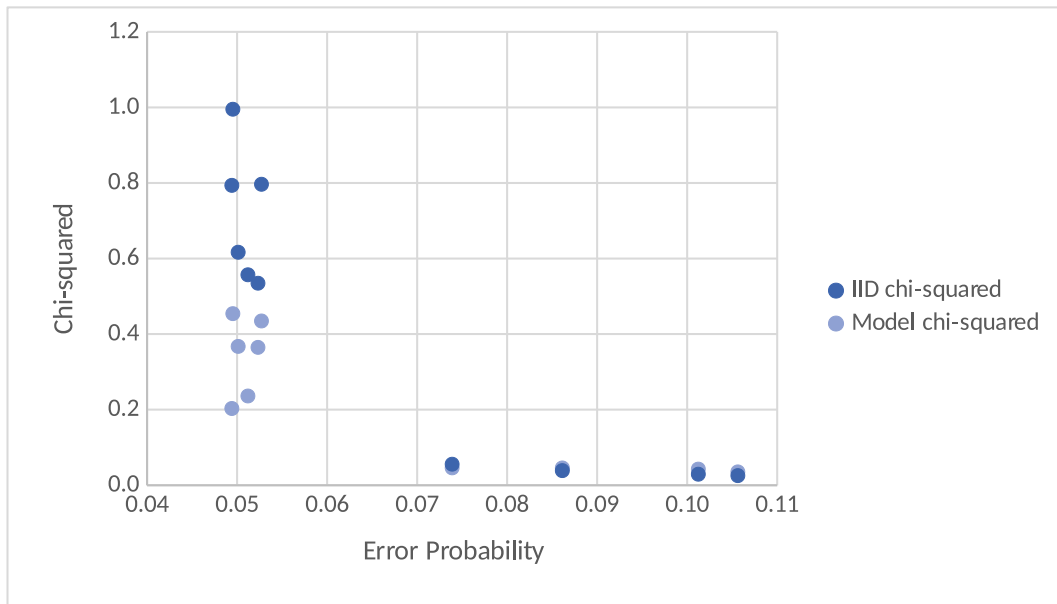
Figure B.1: P_e vs χ^2 for case II with 25% duty cycle interference.
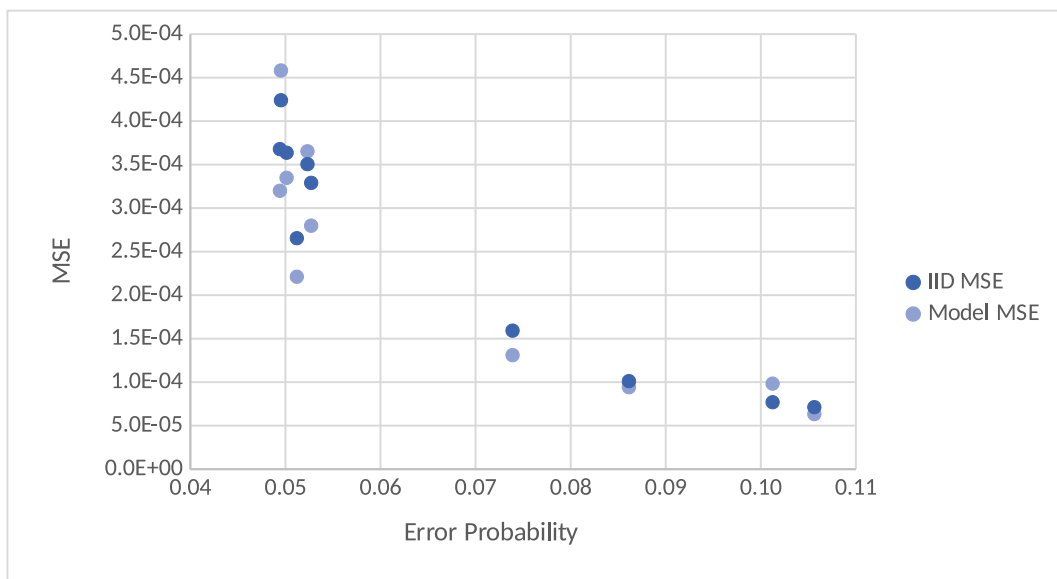
Figure B.2: P_e vs MSE for case II with 25% duty cycle interference.
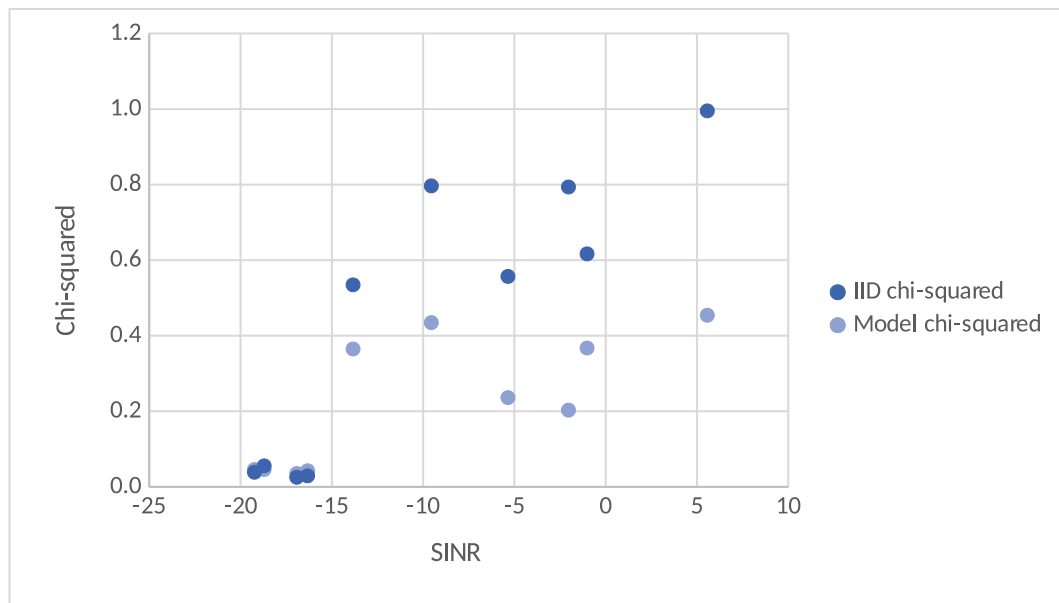
Figure B.3: SINR vs χ^2 for case II with 25% duty cycle interference.
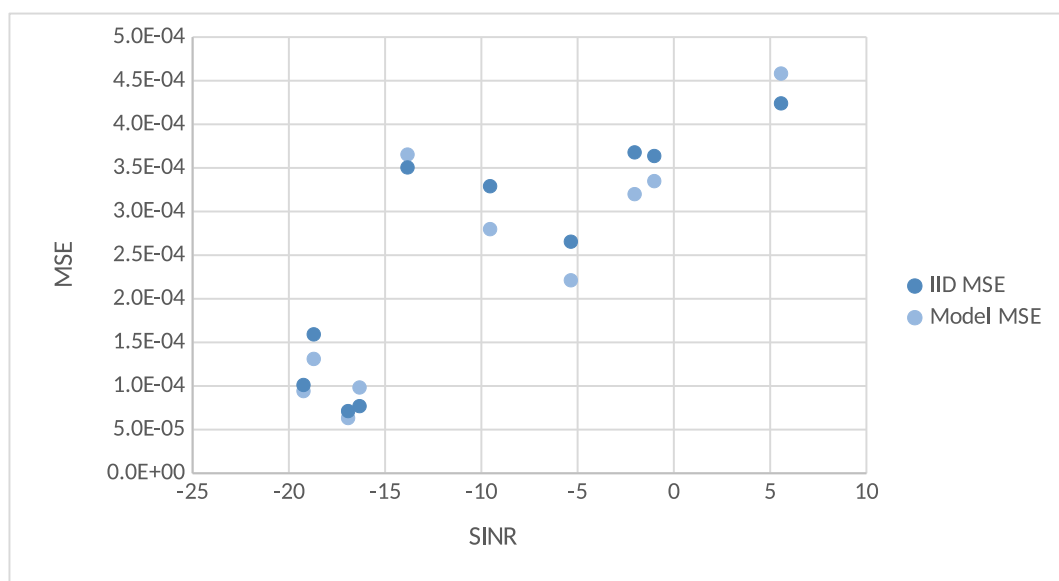
Figure B.4: SINR vs MSE for case II with 25% duty cycle interference.
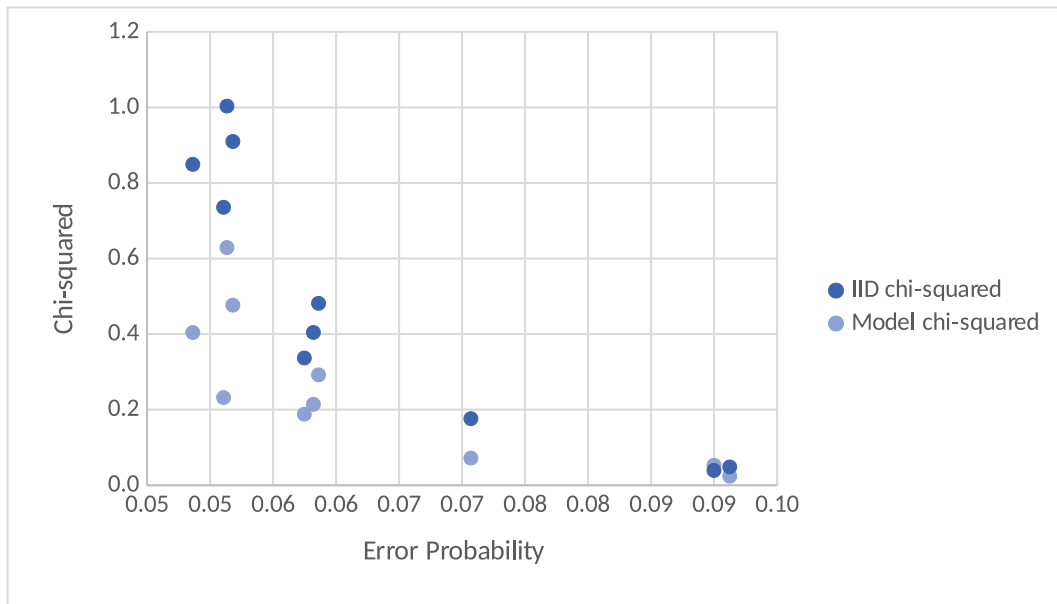
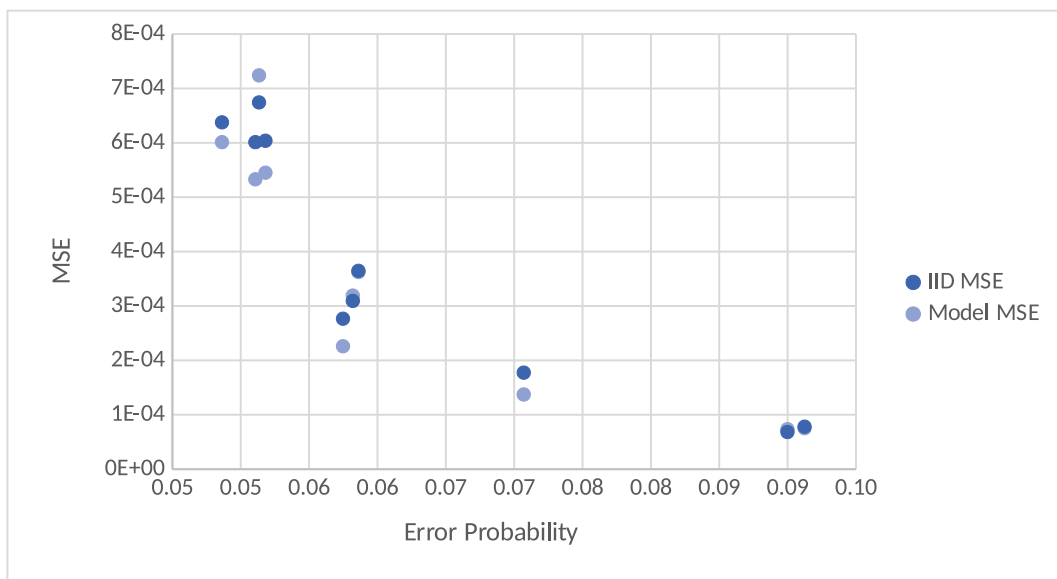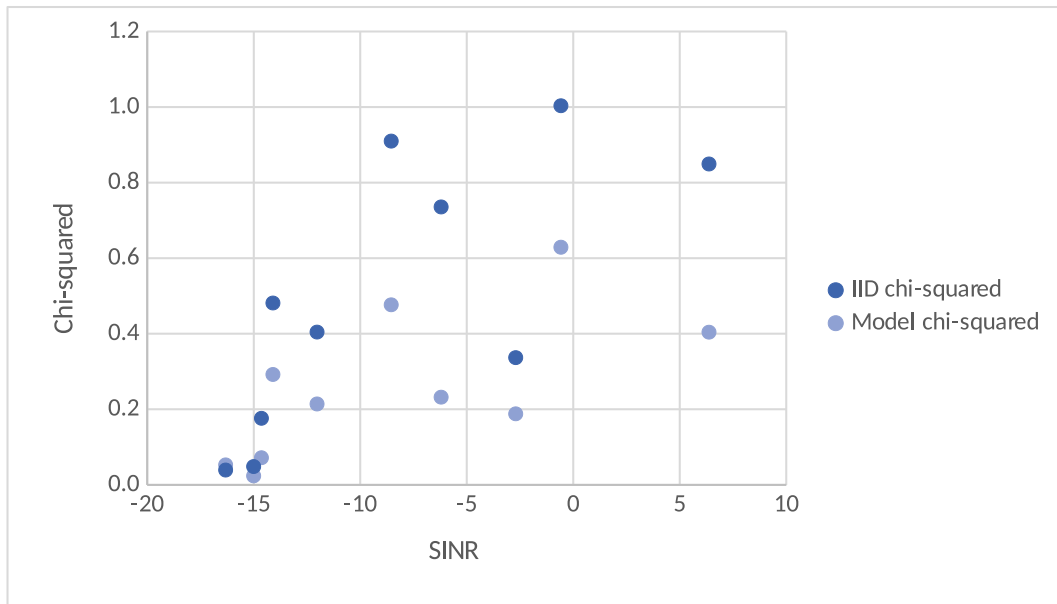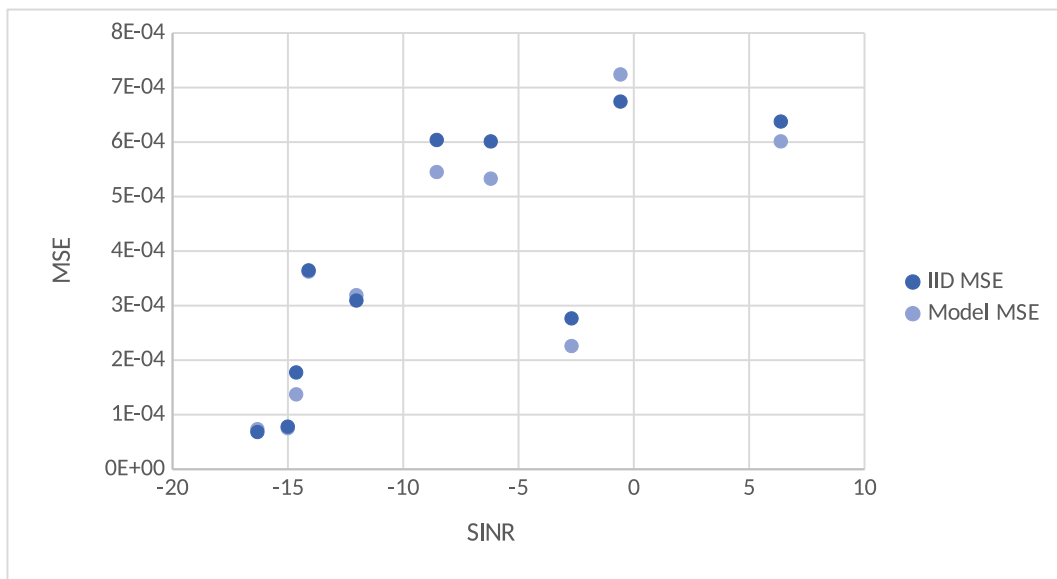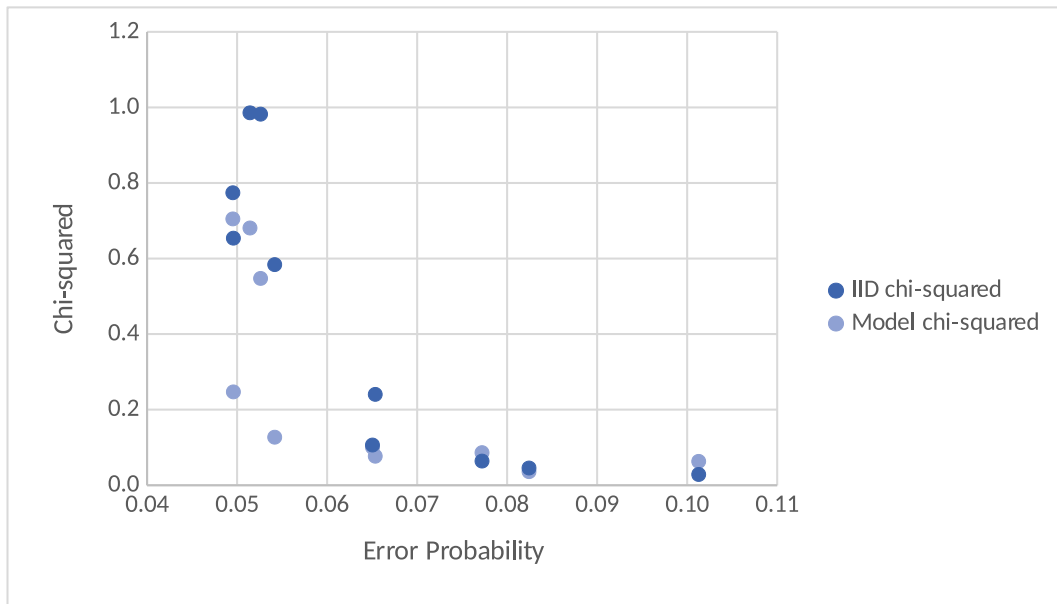**Figure B.5:** P_e vs χ^2 for case II with 50% duty cycle interference.
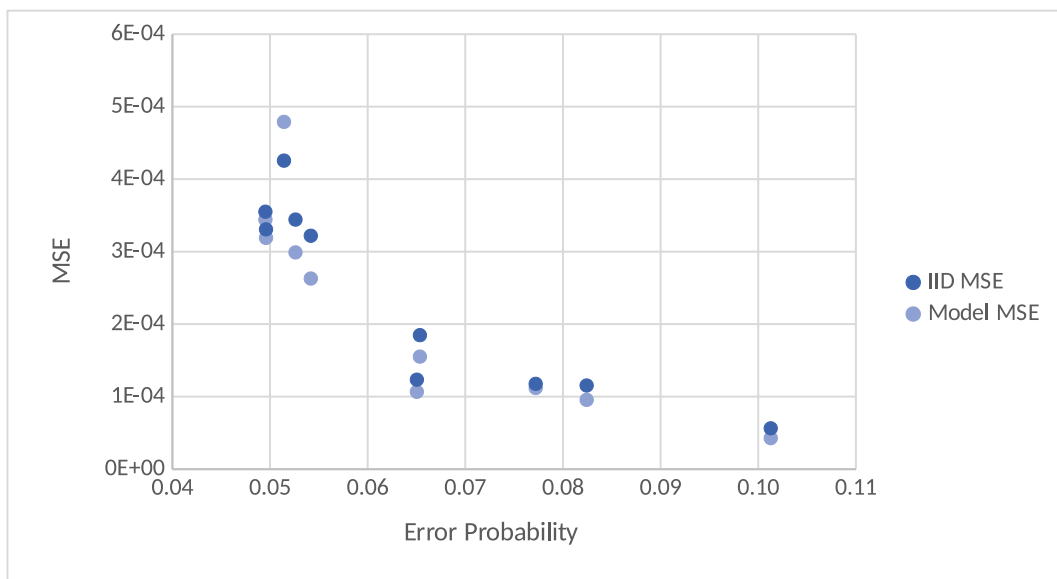

Figure B.6: P_e vs MSE for case II with 50% duty cycle interference.

Figure B.7: SINR vs χ^2 for case II with 50% duty cycle interference.

Figure B.8: SINR vs MSE for case II with 50% duty cycle interference.

Figure B.9: P_e vs χ^2 for case II with 75% duty cycle interference.

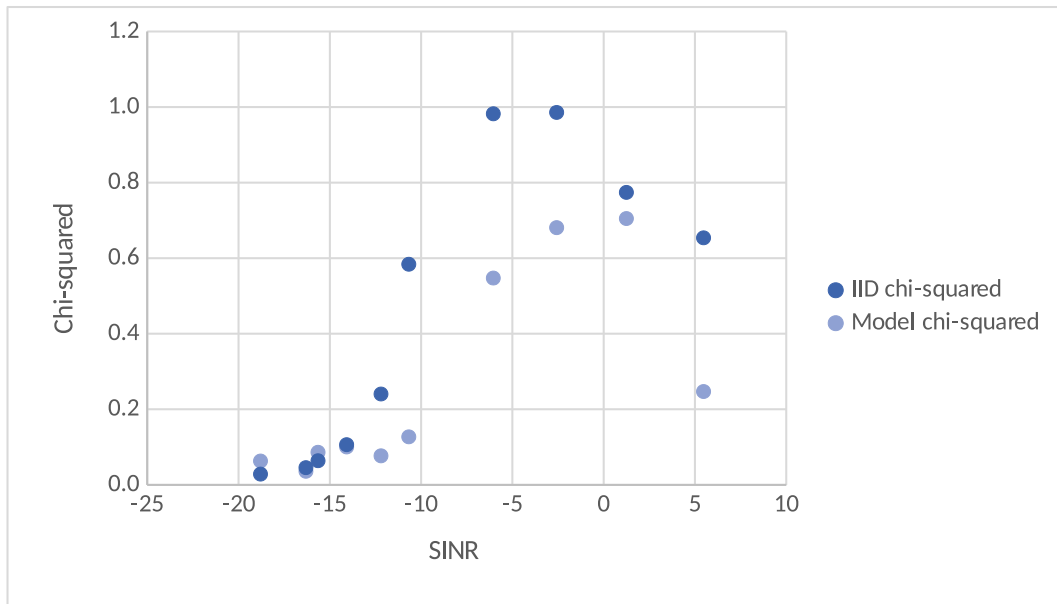**Figure B.10:** P_e vs MSE for case II with 75% duty cycle interference.

Figure B.11: SINR vs χ^2 for case II with 75% duty cycle interference.
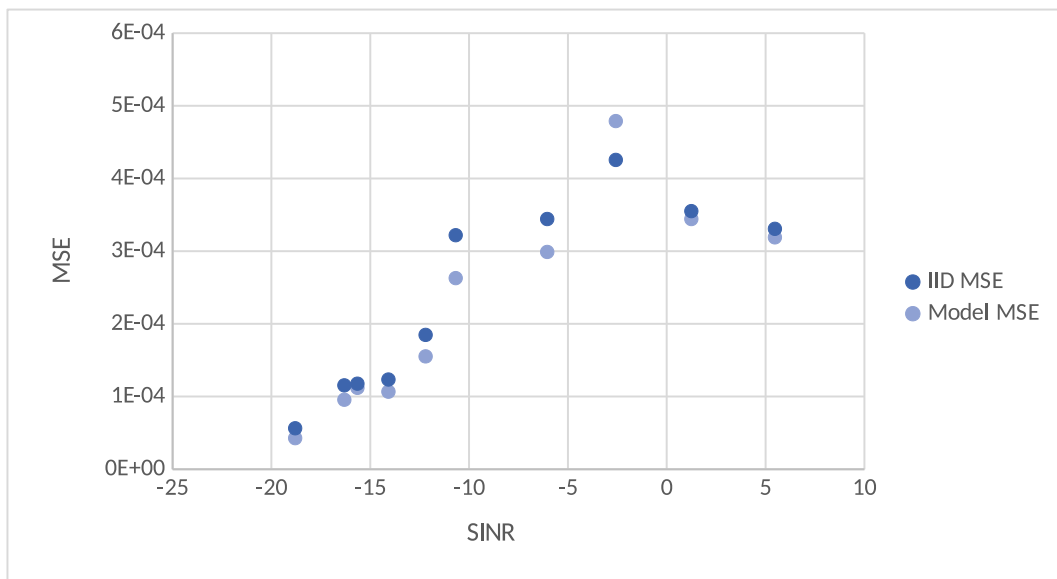

Figure B.12: SINR vs MSE for case II with 75% duty cycle interference.